



Hochschule für Angewandte Wissenschaften Hamburg
Hamburg University of Applied Sciences

Diplomarbeit

Carlos Silvera

Design and Development of a Double-Ridged
Waveguide Horn Antenna

Carlos Silvera

Design and Development of a Double-Ridged
Waveguide Horn Antenna

Diplomarbeit eingereicht im Rahmen der Diplomprüfung
im Studiengang Informations- und Elektrotechnik
Studienrichtung Kommunikationstechnik
am Department Informations- und Elektrotechnik
der Fakultät Technik und Informatik
der Hochschule für Angewandte Wissenschaften Hamburg

Betreuender Prüfer : Prof. Dr. Ing Ralf Wendel
Zweitgutachter : Prof. Dr. Ing Jürgen Missun

Abgegeben am 14. Oktober 2011

Carlos Silvera

Thema der Diplomarbeit

Entwurf und Entwicklung einer Double-Ridged Waveguide Horn Antenne.

Stichworte

Hohlleiter, Simulation, CST Microwave Studio, Hornstrahler, Reflexionsfaktor, Richtwirkung.

Kurzzusammenfassung

Diese Arbeit befasst sich mit einer Double Ridged Waveguide Antenne, die in CST Microwave Studio simuliert wurde und zukünftig gebaut werden soll. Ein Grund hierfür sind die emmensen Preise kommerzieller Antennen, so dass man den Versuch startet eine Antenne für Universitäten herzustellen, die hauptsächlich Forschungs- und Unterrichtszwecken dienen soll. Alle Schritte und Prozesse, die für die Herstellung sowie Optimierung der Antenne notwendig sind, werden im Folgenden gut dokumentiert, so dass der Leser die Möglichkeit bekommen würde diese nachzubauen.

Die konstruierte Antenne hat einen niedrigen VSWR und Reflexionsfaktor mit einem hohen Gewinn. Sie besitzt eine hohe Bandbreite von 0.5 GHz bis 2.67 GHz.

Carlos Silvera

Title of the paper

Design and Development of a Double-Ridged Waveguide Horn Antenna.

Keywords

Waveguide, Horn, CST, reflection factor, directivity, simulation, coaxial cable, ridges.

Abstract

This thesis designs a Double-Ridged Waveguide in the CST Microwave Studio environment that should be constructed in the near future. The high price of commercial antennas is in many cases an obstacle for universities to obtain one for research and education purposes. The whole steps and process of designing and optimizing are well documented to give the reader the opportunity to learn how it is done. The antenna designed in this thesis possesses a low VSWR across its operational frequency band. It has a high and uniform gain and radiation pattern with a very low reflection factor. Its bandwidth from 0.5 GHz to 2.67 GHz meets the requirements set by the university.

Contents

1	Introduction	5
2	Basic Information About Antennas	6
2.1	Electromagnetic field	6
2.1.1	The Maxwell equations	6
2.1.2	Field Regions	7
2.2	Antennas	8
2.2.1	Types of Antennas	8
2.2.2	Antenna Parameters	8
2.2.2.1	Radiation Pattern	9
2.2.2.2	Directivity and Gain	10
2.2.2.3	Bandwidth	11
2.2.2.4	VSWR	11
2.2.2.5	Input Impedance	11
2.3	Waveguide Theory	12
2.3.1	Waves in Hollow conducting Tubes	12
2.3.2	Wave Types and Its Modes	14
2.3.3	Wave Propagation above the Cut-off Frequency	16
2.3.4	Technical designs for the Waveguide	17
2.3.5	Double Ridge Waveguide	18
2.3.6	Coaxial Cable Connection to waveguide	19
2.4	Double Ridged Waveguide Horn	19
2.4.1	Pyramidal Horn	19
3	Designing the Antenna	21
3.1	Waveguide	21
3.1.1	Dimensions	21
3.2	Waveguide with Ridges	26
3.3	Waveguide with Ridges and Feeding Point	29
3.3.1	Optimization With a Back Chamber	34
3.3.2	Optimization With the Help of Microwave Office (AWR Design Environment)	34
3.3.3	Other Methods of Optimization	39
3.4	Waveguide with Ridges and Horn	41
3.4.1	Integration of the Waveguide and Horn	42
3.4.2	Finished Model and its Dimensions	44
4	Measurements and Simulation	48
4.1	Antenna Characteristics	48
4.2	Comparison with the Lindgren 3119	55
5	Conclusion and Further Work	58
	References	59

List of Tables

1	Field Regions	7
2	VSWR to reflection factor	11
3	Wave modes	24
4	$d = 0.1*b$	27
5	$d = 0.15*b$	28
6	$d = 0.25*b$	28
7	S11 and Ground Mode Depending on Position of the Feeding Point	32
8	S11 and Ground Mode Depending on Position of the Feeding Point	33
9	Reflection Factor With one Variable Diameter	38
10	Dimensions for the Complete Model	47

List of Figures

1	3-D Radiation Pattern of a Horn Antenna	9
2	Polar Pattern	9
3	Rectangular waveguide	13
4	Representation of a plane wave on a waveguide wall at high frequency	13
5	TE_{10} Field Distribution	15
6	Field distribution H_{20}	15
7	Field Distribution H_{30}	16
8	Field Distribution H_{01}	16
9	Wavelength limit for rectangular cross-section	17
10	Waveguide with Ridges	18
11	Dimension of a Pyramidal Horn	19
12	Normed Gain from the E and H sector Horn as Function from (B, ρ_0) and (A, ρ_H) .[10]	20
13	Maximum Gain reached by a Horn antenna with specific characteristics	20
14	Waveguide construction 1	22
15	Ground Mode H_{10} in a Waveguide with no Ridges	25
16	Stimulated Wave Modes in a Waveguide	26
17	Second Mode being stimulated	27
18	Stable Frequency Area of Ridged Waveguide	28
19	Design of the Feeding Point in CST-Studio	29
20	Waveguide model with panel jack 1	30
21	Reflexion factor 1	30
22	Smith chart, reflection factor 1	31
23	Waveguide Model with Back Chamber	34
24	Representation of a Coaxial Cable	35
25	Waveguide Representation in AWR Design Environment	35
26	Different Feeding Levels of Port 1	36
27	Representation of p2 in AWR	36
28	Schematic with Coaxial Lines	36
29	Smith Diagram for the Optimized Coaxial Dimension	37
30	Reflection Factor in dB for the Optimized Coaxial Dimension	37
31	Reflection Factor in dB in CST after Coaxial Optimization	39
32	Reflection Factor in Smith in CST after Coaxial Optimization	39
33	Reflection Factor in dB After first Optimization in the Ridges	40
34	Reflection Factor in Smith After First Optimization in the Ridges	40
35	Waveguide Model with Changes in the Ridges	40
36	Reflection Factor for the Finished Waveguide	41
37	VSWR from the Finished Waveguide	41
38	Model of a Simple Horn Antenna	42
39	Gain of the Experimental Horn	42
40	Reflection Factor in Smith for the Experimental Horn Antenna	42
41	Curvature of the Horn Ridges	43
42	Waveguide from the Side	44
43	Waveguide from the Front	45
44	Coaxial Feeding Point	45
45	Complete Model from the Side	46

LIST OF FIGURES

46	Complete Model from the Front	46
47	Directivity at 0.5 GHz	48
48	Directivity at 1 GHz	48
49	Directivity at 1.5 GHz	49
50	Directivity at 2 GHz	49
51	Directivity at 2.5 GHz	49
52	E-Plane at 0.5 GHz	50
53	E-Plane at 1 GHz	50
54	E-Plane at 1.5 GHz	51
55	E-Plane at 2 GHz	51
56	E-Plane at 2.5 GHz	51
57	H-Plane at 0.5 GHz	52
58	H-Plane at 1 GHz	52
59	H-Plane at 1.5 GHz	53
60	H-Plane at 2 GHz	53
61	H-Plane at 2.5 GHz	53
62	Directivity in the Frequency Range 0.4-2.8 GHz	54
63	VSWR from the Complete Model	54
64	Reflection Factor from the Complete Model in dB	55
65	Reflection Factor from the Complete Model in Smith Diagram	55
66	Directivity Comparison between Thesis's Antenna and Lindgren 3119	56
67	VSWR from the Lindgren 3119	56
68	VSWR from Complete Model in the Range from 0.4 to 6 GHz	57
69	Further Changes for the Antenna	58

1 Introduction

Since the first demonstration of wireless technology in 1886 by Heinrich Hertz and its first practical radio application by Guglielmo Marconi in 1901, the antenna has been a key building block in the construction of wireless communications systems. Antennas are used by humans in a daily bases, for example for communication, orientation, warfare and research. Since the days of Hertz, antennas have advanced from a simple wire dipole to more complex structures such as helical antennas, parabolic reflectors, Yagis, microstrip patch arrays, Double-ridged waveguide horns. The use of double-ridged waveguide horn antennas continues to increase. These systems are commonly employed in different fields such as reflector feeds, radar, electronic warfare, detection systems, EMC testing and satellite tracking systems. Very little is known about the already existing antennas in the market. The high price of commercial antennas is in many cases an obstacle for universities to obtain one for research and education purposes. The goal of this thesis is to model a double-ridged waveguide horn antenna with a bandwidth from $0.4GHz$ to $2.5GHz$ with CST Studio to be built in the near future and used for learning purposes at the HAW Hamburg. CST Studio is a professional simulation tool that allows simulations with a vast variety of conditions, excitements and configurations. Literature about modeling this type of antennas is very scarce and no standardized way of modeling them exists. Because of this, the task of modeling the antenna involves extensive systematical experimenting, as well as the use of optimizing methods found in recent literature. It also includes new methods that are implemented in this work.

The task is divided into two mayor steps. In the first step, the waveguide is designed to meet the bandwidth and reflection factors requirements. To extend the maximum practical bandwidth, ridges are introduced in the waveguides to decrease the cut-off frequency of the dominant propagating mode. The introduction and optimization of the coaxial feeding point through various methods follows this process. After the waveguide is completed, the horn is introduced to the structure. The horn also undergoes a series of optimizations, giving it very good results for its directivity, VSWR and reflection factor. Ridges with an exponential curvature are introduced in the horn to make a smooth impedance transition between the feeding point and the free space. At the end, the whole antenna is simulated and compared with the Lindgren 3119. The Lindgren 3119 is a double ridged waveguide antenna with similar characteristics as the one modeled in this thesis.

2 Basic Information About Antennas

This chapter explains some of the crucial elements to understand the functionality of this antenna, starting with electromagnetic fields in Section 2.1. Section 2.2 explains some general aspects from antennas, focusing on the horn antenna. Finally this chapter is engaged with the waveguide theory.

2.1 Electromagnetic field

2.1.1 The Maxwell equations

The Maxwell equations describe not only the formation but also the interaction from electric and magnetic fields, and how electric charges and electric currents act as sources for these. All the field simulation programs base their calculations on the following equations:

- Ampere's law
- Faraday's law of induction
- Gauss's law for electricity
- Gauss's law for magnetism

Ampere's law relates magnetic fields to electric currents. Using this law, it is possible to determine the magnetic field associated with a given current, or the current associated with a given magnetic field. It states that the line integral of the magnetic field around a closed loop is proportional to the electric current flowing through the loop.

$$\oint_{\partial V} \vec{H} \cdot dS = \int_A j_I \cdot dA + \frac{d}{dt} \left(\int_A \vec{D} \cdot dA \right) \quad (1)$$

The Faraday law states that a change of the magnetic field \vec{B} on an area dA over a time dt , induces an electric field \vec{E} .

$$\oint \vec{E} \cdot ds = - \left(\frac{d}{dt} \left(\iint_A \vec{B} \cdot dA \right) \right) \quad (2)$$

Gauss's law for electricity gives a connection between the divergence of the displacement density \vec{D} and the charge density ρ . The electric flux out of any closed surface is proportional to the total charge enclosed within the surface.

$$\oint_{\partial V} \vec{D} \cdot dA = \int_V \rho dV \quad (3)$$

Gauss's law for magnetism says that the magnetic flux from any closed surface is equal to zero when the magnetic field does not have a source.

$$\oint_{\partial V} \vec{B} \cdot dA = 0 \quad (4)$$

2.1.2 Field Regions

The fields surrounding an antenna are divided into 3 main regions:

- Far Field or Fraunhofer Region
- Near Field or Fresnel Region
- Reactive Near Field Region

Table 1: Field Regions

Near Field	Fresnel Region	Far Field
$R < 0.62\sqrt{\frac{D^3}{\lambda}}$	$0.62\sqrt{\frac{D^3}{\lambda}} < R < \frac{2D^2}{\lambda}$	$R < \frac{2D^2}{\lambda}$

These 3 fields are distinguish based on the wavelength that is being analyzed. Table 1 shows the parameters of each field. D is the maximum linear dimension of the antenna, and R is the distance.

The far field region is the most important, since it determines the antenna's radiation pattern. Also, antennas are used to communicate wireless from long distances, so this is the region of operation for most antennas[2]. The far field is defined as the region outside the near-field region, where the angular field distribution is essentially independent of distance from the source. E-field and H-field are in phase, and the field intensity decreases by a factor of $\frac{1}{R}$.

In the Fresnel region is where the radiating fields begin to emerge. The E-field decreases with increasing distance by the factor $\frac{1}{R^2}$.

It is important to take the electric field and the magnetic field separately into consideration in the reactive near field. The reason for this is that they can be as far as 90° phase-shifted. Another reason is that the electric field decreases with increasing distance by the factor $\frac{1}{R^3}$, and the Magnetic field by a factor $\frac{1}{R^2}$.

2.2 Antennas

The IEEE Standard Definitions of Terms for Antennas defines the antenna as “ a means for radiating or receiving radio waves”. In other words, the antennas are devices designed with the objective of sending or receiving electromagnetic waves. Antennas can be divided into two types, transmitting antenna which convert voltage into electromagnetic waves and receiving antenna which do the opposite.

2.2.1 Types of Antennas

There are many kinds of antennas that can be categorized into 10 mayor groups:

- **Linear wire antennas:** ex. small dipole, finite length dipole, Half-wavelength dipole
- **Loop antennas:** ex. small circular loop, circular loop of constant current.
- **Broadband dipoles:** ex. bi-conical antenna, Cylindrical dipole, folded dipole.
- **Broadband antennas:** ex. helical antenna, electric magnetic dipole, Yaqui-uda antenna.
- **Aperture antennas:** ex. circular and rectangular aperture antennas.
- **Horn antennas:** ex. circular reflection feeds, radars, electronic warfare, satellite tracking systems.
- **Micro-strip antennas**
- **Reflector antennas**
- **Smart antennas**

Choosing which antenna to work with depends on many factors. The most important factor is the wave length which determines the antenna’s size. Longer wave lengths (lower frequency) normally require bigger antennas. The dimensions of a broadband antenna depend on its cut-off frequency. Another important factor for choosing a type of antenna is the desired radiation direction. The operating medium (i.e outdoors, indoors) of the antenna is also crucial.

2.2.2 Antenna Parameters

Antennas are key elements for wireless communication. In order to work properly, antennas have to meet specific requirements like a good efficiency, connection properties, and radiation pattern. Sub-chapter 2.2.2.1 explains these characteristics.

2.2.2.1 Radiation Pattern The radiation pattern of an antenna is defined as “a mathematical function or graphical representation of the radiation properties of the antenna as a function of space coordinates. In most cases, the radiation pattern is determined in the far field region and it is represented as a function of the directional coordinates. Radiation patterns include power flux density, radiation intensity, field strength, directivity phase or polarization.”[3] Figure 1 shows a typical radiation pattern in 3-D for a horn antenna. In the pattern it is possible to see the main lobe which is the one coming out in front of the horn colored in red, meaning that this region has the strongest gain. Some side lobes which are in all four sides of the horn colored in green can be differentiated as well as some back lobes.

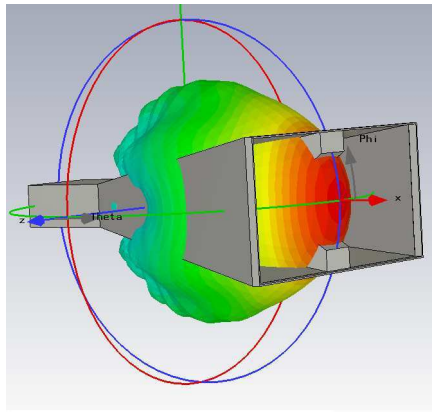


Figure 1: 3-D Radiation Pattern of a Horn Antenna

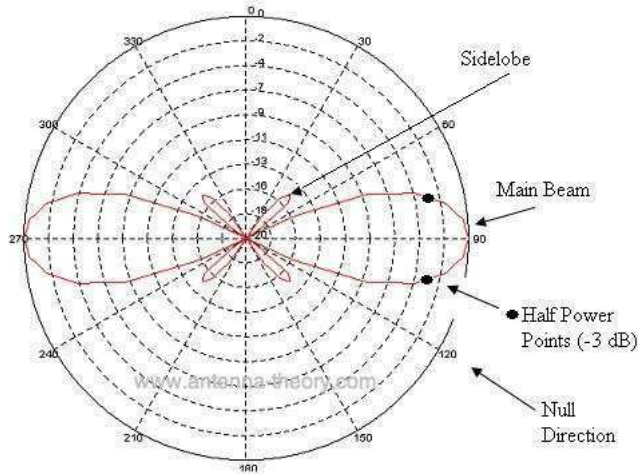


Figure 2: Polar Pattern

The polar patter from the figure above shows a two dimensional pattern where one can also see the main and the side lobes. Another aspect that is displayed in the graphic is the Half Power Beam width (HPBW), which is defined by

IEEE as: “In a plane containing the direction of the maximum of the beam, the angle between the two directions in which the radiation intensity is one-half value of the beam.” This represents a depression of -3dB from the peak of the main beam in a logarithmic scale. The main lobe is represents the directional dependence of the strength of the radio waves from the antenna, and the side lobes usually represent the radiation in unwanted directions.

2.2.2.2 Directivity and Gain Directivity is defined by the IEEE Standard Definition of Terms for Antennas, as “the ratio of the radiation intensity in a given direction from the antenna to the radiation intensity averaged over all directions. The average radiation intensity is equal to the total power radiated by the antenna divided by 4π . If the direction is not specified, the direction of maximum radiation intensity is implied.” With the directivity characteristics and the directivity diagrams it is possible to determine the strength with which the antenna bundles the radiation on a sector. The directivity expresses how stronger the analyzed antenna radiates in a given direction than the reference antenna. Normally an isotropic radiator is taken as reference antenna because of its property of radiating homogeneously in all directions. The formula [4]for the directivity is

$$D = \frac{U}{U_0} = \frac{4\pi U}{P_{rad}} \quad (5)$$

- D = directivity (dimensionless)
- U = radiation intensity (W/ unit solid angle)
- U_0 = radiation intensity of isotropic source (W/ unit solid angle)
- P_{rad} = total radiated power (W)

Another useful measure describing the performance of an antenna is the gain. Although the gain of the antenna is closely related to the directivity, it is a measure that takes into account the efficiency of the antenna as well as its directional capabilities. Directivity only describes the directional properties of the antenna, and it is therefore controlled only by the pattern.

Gain of an antenna (in a given direction) is defined as “the ratio of the intensity, in a given direction, to the radiation intensity that would be obtained if the power accepted by the antenna were radiated isotropically. The radiation intensity corresponding to the isotropically radiated power is equal to the power accepted (input) by the antenna divided by 4π .”[5] Gain is defined as:

$$G = \frac{4\pi U(\theta, \phi)}{P_{in}} (dimensionless) \quad (6)$$

$$g(dB) = 10 * \log(G)$$

Calculating the gain is very complicated, that is why it is mostly done with a special measurement techniques or with simulation software.

2.2.2.3 Bandwidth The bandwidth of the antenna is defined as “the range of frequencies within which the performance of the antenna, with respect to some characteristic, conforms to a specified standard.” [6] The bandwidth is the frequency sector in which the electrical signals are transported with an amplitude declination of no more than 3dB. The bigger the bandwidth, the more information you can theoretically send in one unit of time. In the broadband antennas field, it is usual to express the bandwidth as the ratio of the upper-to-lower frequencies. For example, a 5:1 bandwidth means that the upper frequency 5 times bigger is as the lower.

2.2.2.4 VSWR Voltage standing wave ratio is the optimal power output with the same wave impedance from generator and load. In this case the antenna is the consumer. With an optimal impedance matching you can get a VSWR of 1. In this case a reflection factor of 0% is reached. With no impedance matching a so called “standing wave” is formed which happens when two waves that travel in opposite directions with the same frequency and amplitude meet. This makes the wave change its amplitude from positive to negative and it can make it bigger or smaller. It is also possible to calculate the reflection factor with the VSWR.

$$\Gamma = \frac{VSWR - 1}{VSWR + 1} \quad (7)$$

On the following Table the standing wave proportion to the reflection factor is showed. An optimal result for an antenna is to have a VSWR between 1 and 2.

Standing wave proportion	Reflection factor
VSWR	Γ in %
1	0
2	11
3	25
4	36
5	44
10	67
100	96

Table 2: VSWR to reflection factor

2.2.2.5 Input Impedance Input impedance is defined as “ the impedance presented by an antenna at its terminals or the ratio of the voltage to current at a pair of terminals or the ratio of the appropriate components of the electric to magnetic fields at a point.” [7] To reduce signal reflections, it is important to have a matched connection. This means that the input impedance of the inputs, the characteristic impedance of the transmission line, and the load impedance all have to be equal in order to achieve maximum energy transfer between a wire or coaxial transmission line and an antenna. If the two impedance do not match, a reflected wave will be generated at the antenna terminal and travel back towards the energy source. This reflection of energy results in a reduction in the overall system efficiency.

2.3 Waveguide Theory

The transmission from high frequency signals with metal cables is limited by the so called skin effect. Electricity traveling inside a cable always takes the path with less resistance. With the current flow, a magnetic field is created building a back tension because of the induction. This back tension is dependent from the frequency. The current is pressed against the outer walls by this back tension producing high losses which are too big in frequencies in the microwave range so that these types of cables can only be used for short distances. This is not an option for high performance signals used for example in Radars. It is here when the so called waveguides are used. Waveguides are hollow metallic tubes with a quadratic or circular form in which waves with a particular wavelength travel with light speed. Only waves with a particular relation with the dimensions of the waveguide are transmitted through them. The most important condition for a wave to be able to travel through a waveguide is that its wavelength is smaller than the cut-off wavelength.

Typical applications for waveguides are:

- Satellites: power supply for the antennas and the receiver-amplifier.
- Radio telescopes: power supply.
- Radars: power supply for the sent and received impulses.
- Microwaves for cooking: connection for the magnetron and the cooking area.
- Particle accelerators: power supply of the accelerator.

2.3.1 Waves in Hollow conducting Tubes

A clear view of the wave propagation on a waveguide at high frequencies with the characteristics of Figure 3 can be seen in Figure 4. For a plane wave with electric field vector E and magnetic field vector H , traveling parallel to the side walls of the waveguide, the angle ν , with which the wave travels along the waveguide, depends on the length of the side a , the frequency and the wavelength in free space (λ_0). This dependence makes it possible to meet the multiple condition requirement [11]

$$\sin \nu = \frac{n\lambda_0}{2a} \quad (8)$$

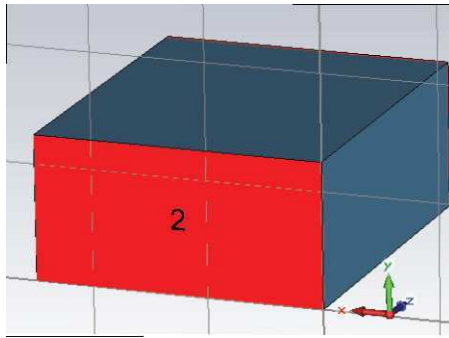


Figure 3: Rectangular waveguide

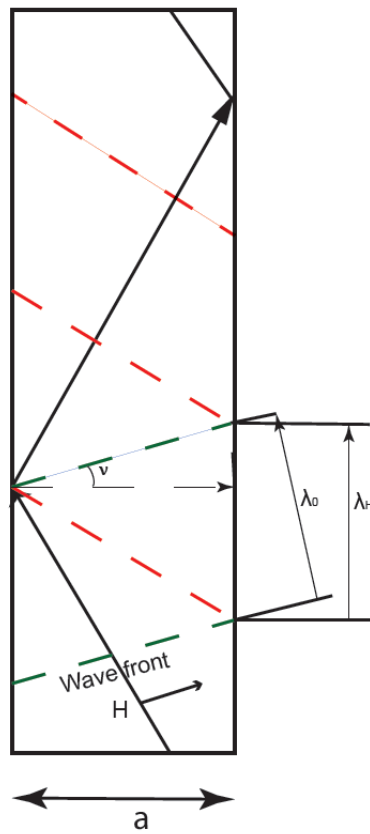


Figure 4: Representation of a plane wave on a waveguide wall at high frequency

Here n is as a whole number in which $n = 1$ represents the ground wave and $n > 1$ describes higher modes. The different types of modes are explained in Subsection 2.3.2. In Figure 4, λ_0 (Wavelength in free space) and λ_H (Waveguide wavelength) are also illustrated. Equation 9 shows the formula for the waveguide wavelength.

$$\lambda_H = \frac{\lambda_0}{\cos \nu} \quad (9)$$

in which

$$\lambda_0 = \frac{C_0}{f} \quad (10)$$

For a bigger λ_0 , ν increases resulting in more frequent reflections on the wall until $\nu = 90^\circ$. At this point, the propagation of waves is impossible and λ_H is infinite. The cut-off frequency at which this phenomenon happens is given by equation 11.

$$\lambda_c = \frac{C_0}{f_c} \quad (11)$$

The cut-off frequency depends on each excited wave type and its modes.

2.3.2 Wave Types and Its Modes

Waveguides have the advantage of high power-handling capability and low loss, but they are expensive and voluminous. There are different types of wave propagation and different types of modes that can exist on transmission lines and waveguides. Transmission lines that consist of two or more conductors may support transverse electromagnetic (TEM) waves, characterized by the lack of longitudinal field components. TEM waves have a uniquely defined voltage, current, and characteristic impedance. Waveguides, often consisting of a single conductor support transverse electric (TE) and/or transverse magnetic (TM) waves, characterized by the presence of longitudinal magnetic or, respectively, field components. [15]

In the type of waveguide handled in this thesis, it is possible to see the TE and the TM waves. The hollow rectangular waveguide can propagate TE and TM modes, but not TEM waves, since only one conductor is present. That is why these two types will be taken into further consideration. Transverse magnetic (TM) waves, also referred to as E-waves, are characterized by $E_z \neq 0$ (Electrical field) and $H_z = 0$ (magnetic field). Transverse electric (TE) waves, also referred to as H-waves are characterized by $E_z = 0$ and $H_z \neq 0$. The ground mode wave is the wave mode with the lowest cut-off frequency. In rectangular waveguides, the ground mode is TE_{10} or H_{10} . Electromagnetic energy with a frequency below the cut-off frequency for that particular mode will be attenuated to a negligible value in a relatively short distance. This grammatical use of cut-off frequency is opposite to the one used for coaxial cable, where cut-off frequency is for the highest useable frequency. [8]

The simplest and most common transmitted wave in a rectangular waveguide is the ground magnetic wave or H_{10} . This mode is called the TE_{10} or transverse electric. It has this name because all electric fields are transverse to the direction of the propagation and has no longitudinal electric field. In general, they are referred to as TE_{mn} . In picture 5 the field distribution in a H_{10} wave can be observed. It is clear that the maximum energy from the fields are concentrated in the middle.

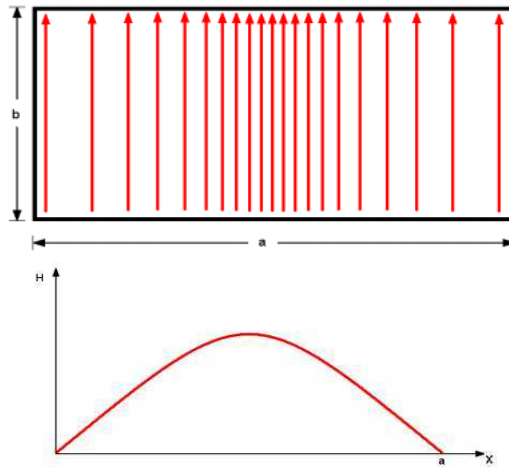


Figure 5: TE_{10} Field Distribution

The m indicates the number of half wave loops across the height of the waveguide, in this case 1, and the n indicates the number of half wave loops across the width of the waveguide, in this case 0. To be able to understand this better there are some examples below where the waves H_{20} , H_{30} , H_{01} are shown.

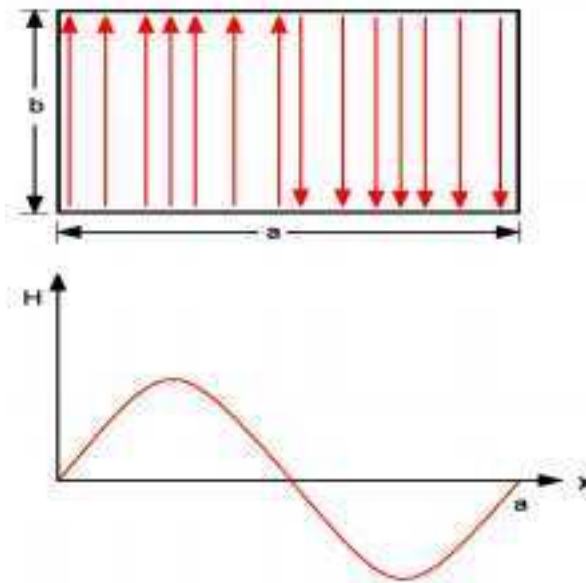


Figure 6: Field distribution H_{20}

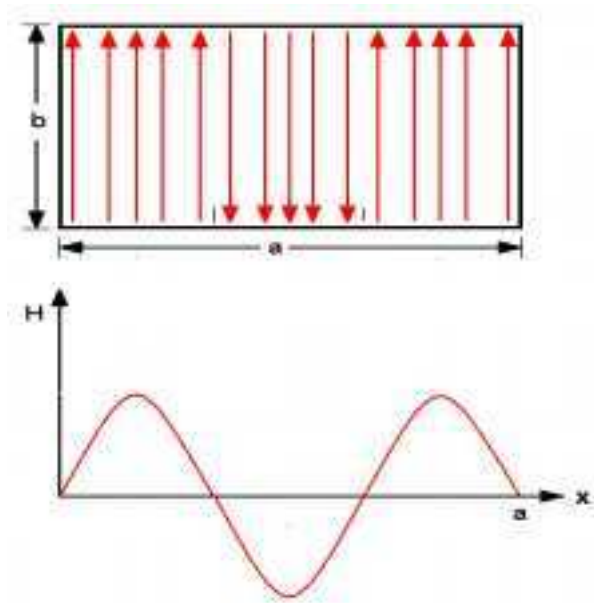


Figure 7: Field Distribution H_{30}

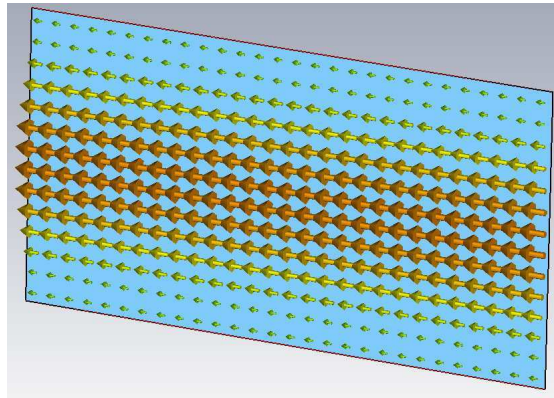


Figure 8: Field Distribution H_{01}

2.3.3 Wave Propagation above the Cut-off Frequency

If an oscillation in a hollow waveguide is stimulated with a frequency $f > f_c$, it is possible for a wave to propagate without attenuation. The resulting waveguide wavelength is

$$\lambda_H = \frac{\lambda_0}{\sqrt{1 - \left(\frac{\lambda_0}{\lambda_c}\right)^2}} \quad (12)$$

Therefore, you can calculate the free space wave length λ_0 with

$$\lambda_0 = \frac{\lambda_H}{\sqrt{1 - (\frac{\lambda_H}{\lambda_0})^2}} \quad (13)$$

Another important factor to know is the field wave resistance. This can be related to the field wave resistance from the free space $Z_0 = \sqrt{\mu_0/\epsilon_0} = 120\pi\Omega = 377\Omega$. Having this, the field wave resistance for H-waves can be calculated with [12]

$$Z_f = \frac{Z_0}{\sqrt{1 - (\frac{\lambda_0}{\lambda_c})^2}} \quad (14)$$

and the E-waves with

$$Z_f = Z_0 \sqrt{1 - (\frac{\lambda_0}{\lambda_c})^2} \quad (15)$$

Upwards to the cut-off frequency is the field wave resistance entirely real, below it, it is entirely inductive.

2.3.4 Technical designs for the Waveguide

The dimensions of a waveguide depend on the operating frequency range. It is important to choose the operating frequency so that it is between the cut-off frequency from the ground mode and the cut-off frequency from the next exited mode. It is essential to do this to avoid disturbances from the other modes. Knowing the cut-off frequency of the ground mode, and the one from the next higher mode, the operating range of the waveguide can be determined. As seen in Figure 9, the optimal proportion is $\frac{b}{a} \approx 0.5$. It is possible to use other proportions, it all depends on the designing technique. The depth of the waveguide does not play a big role in its performance, but the distance from the feeding point to the front of the waveguide does, so the waveguide should not be too short.

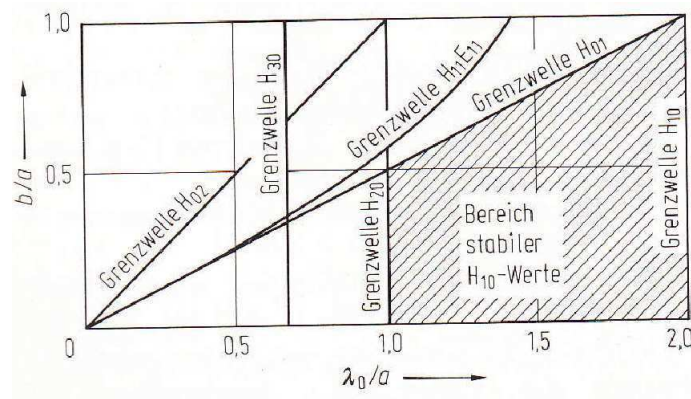


Figure 9: Wavelength limit for rectangular cross-section

2.3.5 Double Ridge Waveguide

A common way to increase the bandwidth of a waveguide is to introduce ridges in the middle of the waveguide that go along the propagation direction. Although the increase is significant, it happens at the expense of higher attenuation and lower power-handling capability. “Introduction of the ridges mainly lowers the cut-off frequency of the TE mode from that of the unloaded guide, which is predicated on width alone. The reason for this can easily be explained when the field configuration in the guide at cut-off is investigated. At cut-off there is no longitudinal propagation down the guide. The waves simply travel back and forth between the side walls of the guide. In fact the guide can be viewed as a composite parallel plate waveguide of infinite width where the width corresponds to the direction of propagation of the normal guide. The TE mode cut-off occurs where this composite guide has its lowest-order resonant frequency. This occurs when there is only one E field maximum across the guide which occurs at the center for a symmetrical ridge. Because of the reduced height of the guide under the ridge, the effective TE mode resonator is heavily loaded as though a shunt capacitor were placed across it. The cut-off frequency is thus lowered considerably.”[9]

The waveguide is shown in Figure 10 after the introduction of the ridges.

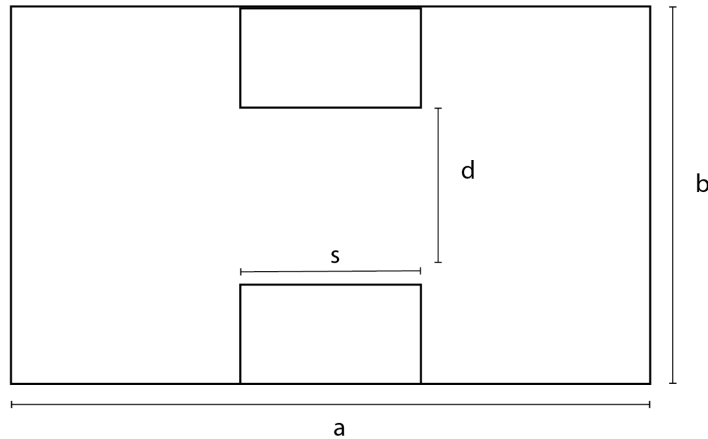


Figure 10: Waveguide with Ridges

There are no defined measurements for s and d . It is very helpful in this stage to use a simulation program to be able to find out the optimal proportion from height to width from the ridges.

2.3.6 Coaxial Cable Connection to waveguide

A very important part of an antenna is its feeding point. In high frequency range, the antenna is often connected to the source with a coaxial cable. The maximum and most efficient transfer of electrical energy occurs when the source impedance is matched to the load impedance. If both characteristic impedance are the same, the energy from the transmitter travels almost without power loss throughout the transmission line into the antenna. The transition between coaxial probe and the double-ridged waveguide is important for the return loss performance of the horn antenna.

2.4 Double Ridged Waveguide Horn

The simplest aperture antenna is the type fed with a H_{10} wave and open at the end with a rectangle form. This kind of antenna is probably the most widely used in the microwave area. There are three kinds of rectangular horns. The H-plane sectoral horn, the E-plane sectoral horn and the pyramidal horn. Like the name suggests, the H-plane sectoral horn flares in the direction of the H-field while keeping the other constant, and the E-plane horn flares in the E-field direction. The horn used in this thesis is the pyramidal horn. This type of horn is described in the following section.

2.4.1 Pyramidal Horn

The radiation characteristics are a combination of the E- and the H-plane sectoral horns. On Figure 11 the dimensions of a pyramidal horn are shown from the perspective of its H-plane.

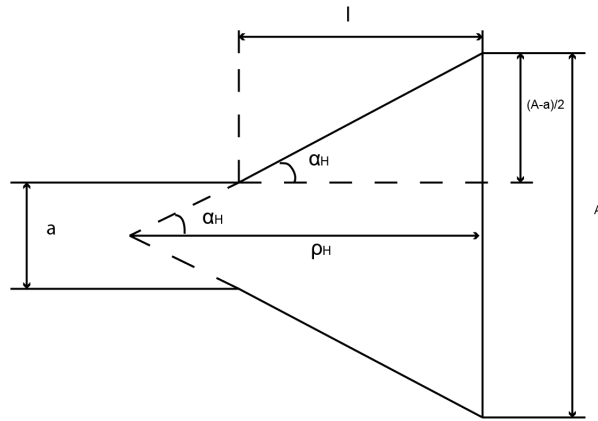


Figure 11: Dimension of a Pyramidal Horn

Equations 16 and 17 are derivated from Figure 11 :

$$\tan \alpha_H = \frac{(A - a)}{(2L)} = A/(2\rho_H) \quad (16)$$

and:

$$\tan \alpha_E = \frac{(B - b)}{(2L)} = B/(2\rho_E) \quad (17)$$

If the angle $\alpha_{H,E}$ is increased and the length L is fixed, then the aperture area and the gain of the antenna will increase. However, when this happens, the phase error in the aperture will also increase leading to an abrupt fall after the maximum values for A and B are achieved. Using the following graphs it is possible to establish the dimensions of a horn depending on the desired gain wanted at the end.

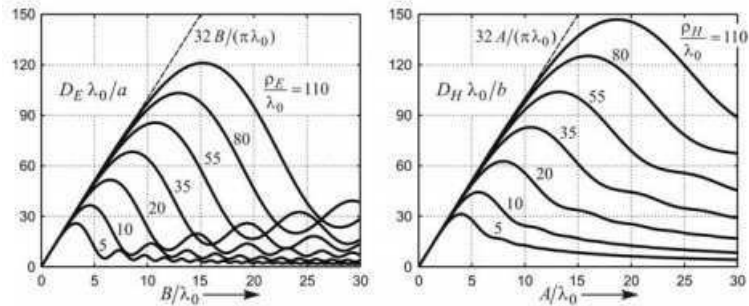


Figure 12: Normed Gain from the E and H sector Horn as Function from (B, ρ_0) and (A, ρ_H) . [10]

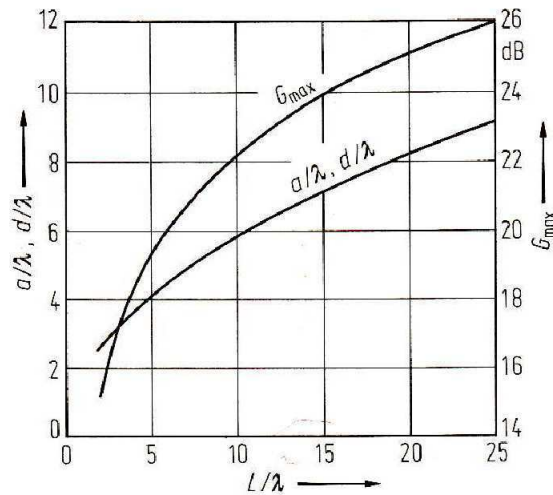


Figure 13: Maximum Gain reached by a Horn antenna with specific characteristics

3 Designing the Antenna

CST Microwave Studio is a specialized tool for the 3D EM simulation of high frequency components. It combines the Perfect Boundary Approximation (PBA) and the Finite Integration Technique (FIT) making it a very powerful simulation software providing a fast and accurate analysis of high frequency (HF) devices such as antennas, filters, couplers, planar and multilayer structures and SI and EMC effects. This software is used in all designing steps of this thesis. The task of constructing the antenna is divided into 4 parts. In Section 3.1 the dimension of the waveguide according to the desired bandwidth of the antenna is established with the help of the cut-off frequencies of each stimulated mode given by the software.

Section 3.2 and 3.3 are about optimizing the waveguide in order to get a wider bandwidth and a reflection-less antenna. Two main adjustments are made here. The first and most important is the addition of ridges inside the waveguide, helping it to expand its bandwidth, and the second one is the optimization of the coaxial cable used to feed the signal into the antenna. The main purpose of these changes is to get an antenna with the least amount of reflection in the widest possible frequency range.

Section 3.4 explains the construction of the horn with its ridges. Simulations are used to find the best possible constellation of length, width and exponential function of the horn.

Finally, all parts are put together Section 3.4.1 to form the double ridged waveguide antenna.

3.1 Waveguide

To start designing the antenna, it is crucial to specify the bandwidth the antenna should have at the end. After the successful design and construction from the antenna, it will be used in the HAW- Hamburg for measuring purposes in the lab, giving the students the opportunity to experiment with antennas with a wider range and a larger power capability. Due to the frequency generator provided by the university, it is certain that the upper frequency range has to be $3GHz$. The frequency generator is the Rohde & Schwarz SME 03 with a frequency range from $5KHz$ to $3GHz$.

The lower frequency was discussed between student and professor and it was established at a range from $0.3GHz$ to $0.8GHz$. This means that the antenna should have a bandwidth anywhere from $0.3GHz$ to $3GHz$.

3.1.1 Dimensions

Knowing the range of the wanted frequency, and according to Equation 11 explained in Section 2.3, it is possible to calculate the dimensions of the waveguide using the following parameters:

- Cut-off frequency $f_c = 400MHz$
- Speed of light in vacuum $C_0 = 299,792,458m/s$

$$\lambda_c = \frac{C_0}{f_c}$$

$$\lambda_c = \frac{299.792.458 \frac{m}{s}}{400MHz}$$

$$\lambda_c = 74.9cm$$

From the theory it is known that $\lambda_c = 2 * a$ and that $a = 2 * b$ so:

$$a = \frac{\lambda_c}{2} = 37.5cm$$

$$b = \frac{a}{2} = 18.75cm$$

With the dimension defined, it is possible to start designing the model. CST Studio is very effective for this purpose. It is just necessary to create a brick with the dimensions mentioned before. The length of the waveguides does not play a big role in the bandwidth or the performance of the waveguide, therefore a random length is chosen as $z = 500mm$.

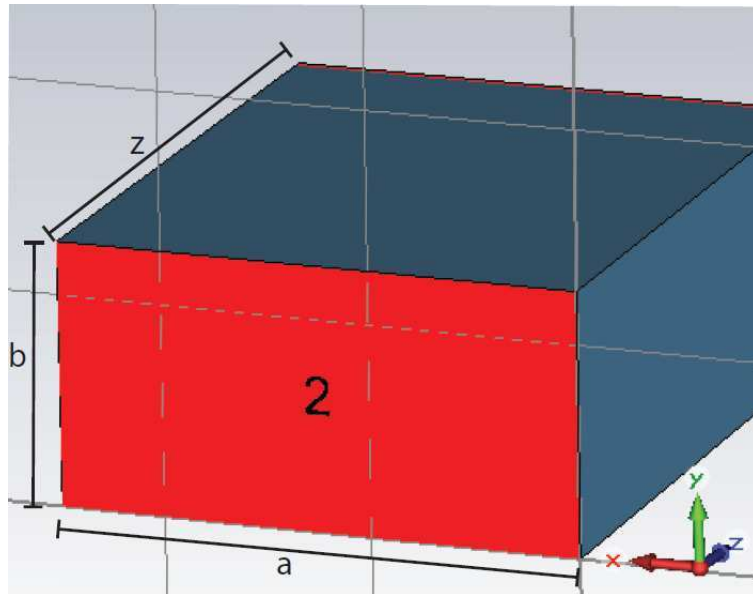


Figure 14: Waveguide construction 1

As shown in the figure, the material from the waveguide is vacuum. This is only used in the first part of the simulation in order to study which modes travel through the waveguide in the desired frequency range. To do this, a few changes are done. First of all, two waveguide ports have to be defined at each end of the waveguide. Each one with a number of 8 modes that should be stimulated. This helps to identify in which frequency range the H_{10} wave can travel undisturbed in the waveguide before one or more other wave modes can be stimulated. The second change is to establish boundary conditions to make the waveguide electrically conductive.

A great advantage from the simulation program is that it returns the cut-off frequency for each mode and shows each mode's type. In the following table, some examples of modes are displayed.

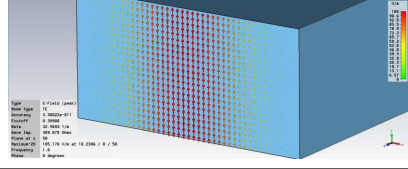
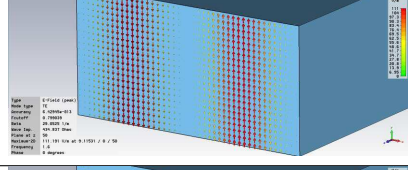
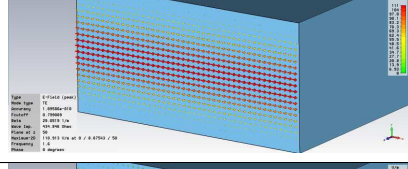
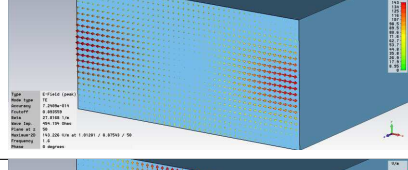



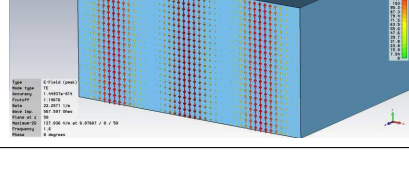
Mode	Electric Field Image	f_c (GHz)	Mode type
H_{10}		0.39988	TE
H_{20}		0.79956	TE
H_{01}		0.79009	TE
H_{11}		0.8935	TE
E_{11}		0.8935	TM
H_{21}		1.13005	TE
E_{21}		1.13005	TM
H_{30}		1.19676	TE

Table 3: Wave modes

Considering the modes and the cut-off frequencies in Table 3, it is possible to detect in which frequency range the ground mode, H_{10} , can travel undisturbed. If the mode H_{10} is observed, it can be seen that its cut-off frequency is at

399MHz . It is possible to detect the next mode that is stimulated because of its symmetry in the middle of the waveguide. In this case it would be the fourth one, H_{30} , with a cut-off frequency of 1.19GHz . This means that the ground mode can travel undisturbed in the range from 400MHz to 1.2GHz . This results do not meet the expectations that this project has established. From the theory mentioned in Section 2.3.5, it is known that with a few changes like adding ridges to the waveguide, the cut-off frequency can be lowered significantly. Therefore the dimensions of the waveguide are calculated again taking into account a larger cut-off frequency so that it can have a wider bandwidth, but still have a cut-off frequency around 500MHz after the optimization.

The new dimensions are calculated with a cut-off frequency from $f_c = 1.2GHz$.

$$\lambda_c = \frac{299.792.458 \frac{m}{s}}{1.2GHz}$$

$$\lambda_c = 24.9cm$$

$$a = \frac{\lambda_c}{2} = 12.45cm$$

$$b = \frac{a}{2} = 6.225cm$$

After redesigning the model, it was once again simulated with 8 modes in each port. On the following figure the ground mode with a cut-off frequency of 1.198GHz can be appreciated.

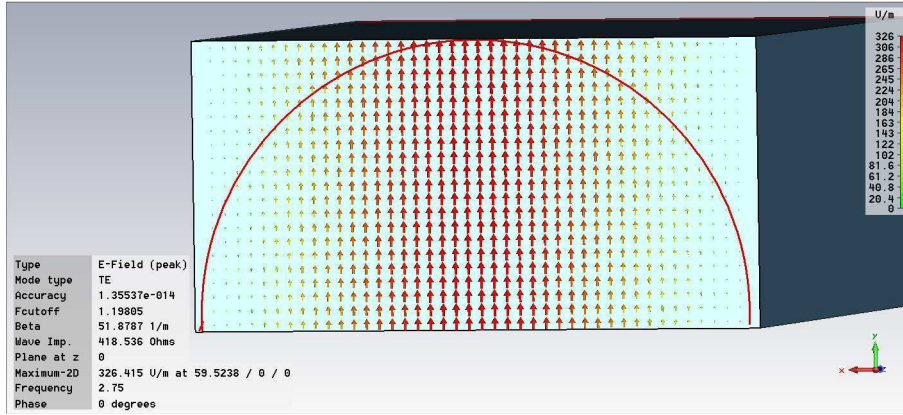


Figure 15: Ground Mode H_{10} in a Waveguide with no Ridges

It is also easy to see in the Figure 15 why this mode a H_{10} is. The electric field has only one component in the y-axis. In this case $E \sim \sin(\frac{x}{a} * 1\pi)$. The next step in the process is to find the next mode that is being stimulated, to see which will be the bandwidth of the waveguide in which the ground mode can travel undisturbed. The next stimulated mode has a cut-off frequency by 2.67GHz . This is demonstrated in Figure 16.

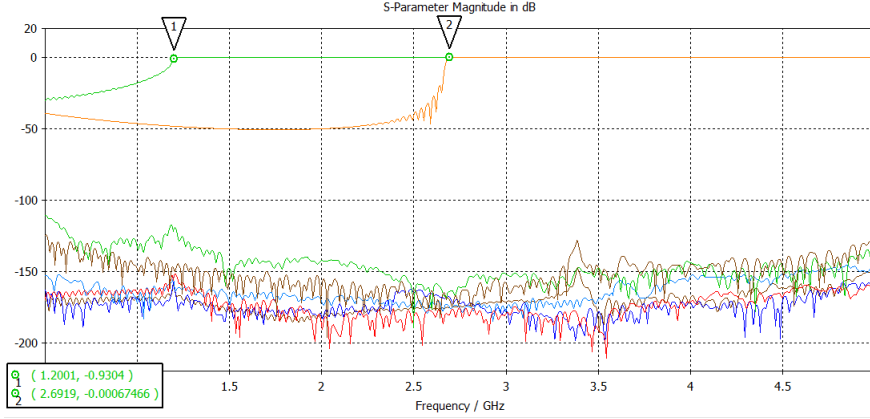


Figure 16: Stimulated Wave Modes in a Waveguide

The ground mode is stimulated with a cut-off frequency of $1.2GHz$ and it goes undisturbed until the next mode is stimulated with a cut-off frequency of $2.67GHz$. On the bottom part of the figure are all of the modes that are not being stimulated at this frequency range.

After doing all this process, the waveguide has a bandwidth of $1.4GHz$ without taking into account the reflexion factor. Although this would be a very large bandwidth for other types of antennas, it is not much for a waveguide.

3.2 Waveguide with Ridges

Once the dimensions of the waveguide are fixed, it is optimized to get the wanted results. It is known from Section 2.3.5 that by introducing ridges into the waveguide that go completely from front to back, the size of the bandwidth can be extended. There is no specific literature for the dimension of the ridges, so it is done systematically.

The goal is to find the ridge dimensions with which the waveguide can have the largest bandwidth for a fixed waveguide width a and height b . The ridge dimensions are defined by their width, s , and the length of half of the space between the ridges, d . Three different cases for different ratios of $\frac{d}{b}$ are defined and simulated for different values of s . The first one is for $\frac{d}{b} = 0.1$, the second one $\frac{d}{b} = 0.15$, and the third one $\frac{d}{b} = 0.25$, meaning that in each case the distance between the ridges is changed. In each case the wavelength ratio of the first and second cut-off frequency is calculated and plotted as shown in Figure 18. The ratio of $\frac{s}{a}$ is plotted in the x-axis while the ratio of the cut-off frequency wavelengths $\frac{\lambda_{c1}}{\lambda_{c2}}$ is plotted in the y-axis.

The resulting model 17 shows an example of how it is possible to recognize which mode is the next one to be stimulated. The symmetry in the middle is very easy to appreciate.

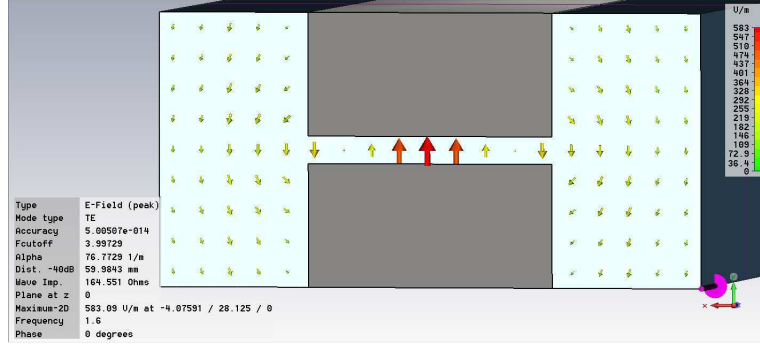


Figure 17: Second Mode being stimulated

The following tables show the cut-off frequencies and corresponding wavelengths for the three different ratios for different values of $\frac{s}{a}$. The first and second cut-off frequencies are computed with help of CST-Microwave Studio.

- $a = 125mm \rightarrow$ Width of the waveguide.
- $b = 62.5mm \rightarrow$ Height of the waveguide.
- s , variable \rightarrow Width of the ridges.
- d , variable \rightarrow Half of the distance between the ridges.
- $f_{c1} \rightarrow$ Cut-off frequency for the ground mode.
- $f_{c2} \rightarrow$ Cut-off frequency for the second mode being stimulated.
- $\lambda_{c1} \rightarrow$ Wavelength from f_{c1} .
- $\lambda_{c2} \rightarrow$ Wavelength from f_{c2} .

$\frac{s}{a}$	f_{c1} (GHz)	f_{c2} (GHz)	λ_1 (cm)	λ_2 (cm)	$\frac{\lambda_1}{\lambda_2}$
0.07	0.6029	2.71	49.76	11.07	4.49
0.1	0.57	2.78	52.63	10.79	4.87
0.2	0.4994	3.05	60	9.84	6.10
0.25	0.4565	3.22	65.72	9.32	7.05
0.3	0.45	3.42	66.67	8.77	7.60
0.4	0.444	3.88	67.57	7.73	8.73
0.45	0.442	4	67.87	7.5	9.05
0.5	0.44	3.89	68.18	7.71	8.84
0.6	0.45	3.44	66.67	8.72	7.64
0.7	0.485	3.07	61.86	9.77	6.32

Table 4: $d = 0.1*b$

$\frac{s}{a}$	f_{c1} (GHz)	f_{c2} (GHz)	λ_1 (cm)	λ_2 (cm)	$\frac{\lambda_1}{\lambda_2}$
0.07	0.691	2.77	43.42	10.83	4.00
0.1	0.656	2.82	45.73	10.64	4.29
0.2	0.585	3.08	51.28	9.74	5.26
0.25	0.5629	3.244	53.30	9.25	5.76
0.3	0.547	3.43	54.84	8.75	6.27
0.4	0.53	3.84	56.60	7.81	7.24
0.45	0.528	3.91	56.82	7.67	7.40
0.5	0.53	3.77	56.60	7.96	7.11
0.6	0.5457	3.22	54.98	9.32	5.90
0.7	0.579	3.05	51.81	9.84	5.26

Table 5: $d = 0.15*b$

$\frac{s}{a}$	f_{c1} (GHz)	f_{c2} (GHz)	λ_1 (cm)	λ_2 (cm)	$\frac{\lambda_1}{\lambda_2}$
0.07	0.801	2.86	37.45	10.49	3.57
0.1	0.779	2.9	38.51	10.34	3.72
0.2	0.693	3.013	42.25	9.96	4.24
0.25	0.678	3.29	43.26	9.12	4.74
0.3	0.669	3.46	44.25	8.67	5.10
0.4	0.66	3.78	44.84	7.94	5.65
0.45	0.663	3.79	45.45	7.92	5.74
0.5	0.68	3.66	45.25	8.20	5.52
0.6	0.7	3.32	44.12	9.04	4.88
0.7	0.719	3.03	41.72	9.90	4.21

Table 6: $d = 0.25*b$

With the values in these tables it is possible to plot the three curves seen in Figure18

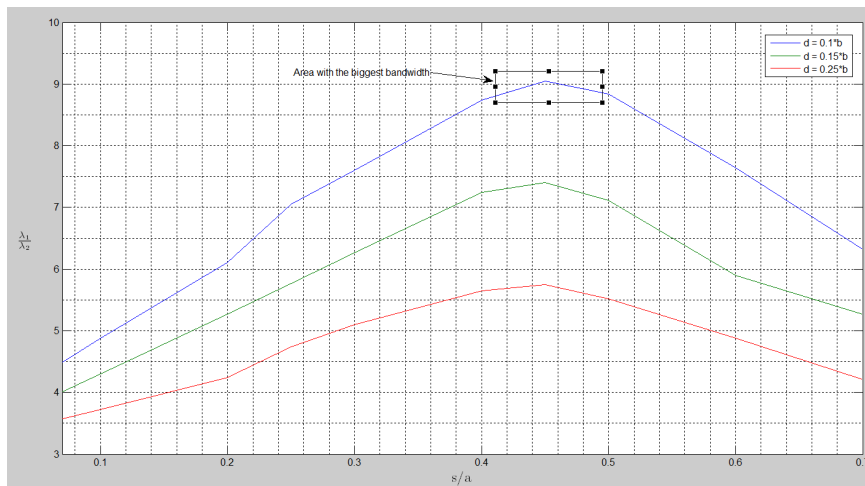


Figure 18: Stable Frequency Area of Ridged Waveguide

This figure is used to find the point on a curve where the relation between cut-off wavelengths is the greatest. This point is where the cut-off frequencies are the most apart, meaning that the bandwidth is the greatest. As shown in Figure 18 the ridge dimension that optimizes the bandwidth is $\frac{d}{b} = 0.1$ where $s \approx 0.45 * a$. This leads to the following ridge dimension:

- $s = 0.45 * a = 0.45 * 125mm = 56.25mm$
- $d = 0.1 * b = 0.1 * 62.5mm = 6.25mm$

After introducing these dimensions into the model, it is feasible to say that the waveguide has a working frequency range in which just one mode is stimulated from 0.44 GHz to 2.38 GHz. This is a very good improvement in comparison to the first model.

3.3 Waveguide with Ridges and Feeding Point

Although a satisfying range in the waveguides' bandwidth is reached with the introduction of the ridges, the antenna is not nearly finished. A very important aspect to be taken into account is the reflection factor. For an antenna to be able to transmit the waves correctly, the reflection factor has to be below -10dB. This section will show how the feeding point is introduced and optimized so that the reflection factor stays under -10dB throughout the desired bandwidth.

The panel jack or feeding point that is used for this antenna is the Rosenberger 53K410-700N5. It is a N connector with a resistance of 50Ω , and a inner diameter (d) of $3mm$ for the transmitting cable. It is designed in CST-Studio as in Figure 19

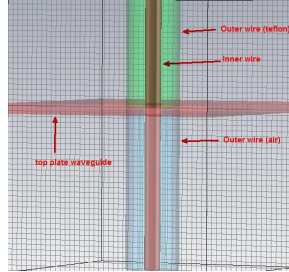


Figure 19: Design of the Feeding Point in CST-Studio

Coaxial cables are made up of the inner wire and the outer wire. The energy or information traveling throughout the coaxial cable should not be affected by outer electromagnetic disturbances, that is why the outer wire also works as a shield against these disturbances. Teflon is used in this case as a dielectric material between the two wires. Teflon has a relative permittivity $\epsilon_r = 2.2$. With an outer diameter (D) of $10mm$ it has a characteristic impedance of

$$\frac{60\Omega}{\sqrt{\epsilon_r}} * \ln \frac{D}{d} = \frac{60\Omega}{\sqrt{2.2}} * \ln \frac{10}{3} \approx 50\Omega$$

This particular panel jack is design so that the Teflon is only on the outer part of the waveguide. On the inside it has air as dielectric material between both

wires. First the outer wire in the outside of the waveguide and on the inside have the same diameter (10mm). Figure 20 shows the model of the waveguide with ridges and panel jack. The feeding point is initially placed randomly in the waveguide.

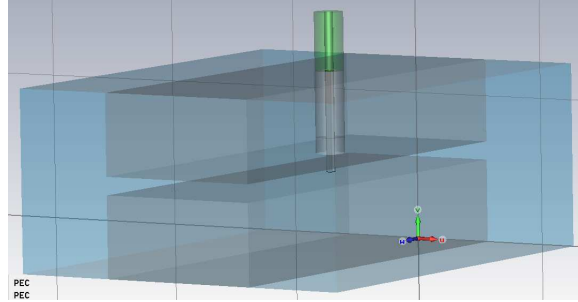


Figure 20: Waveguide model with panel jack 1

Port 1 is then assigned to the top of the panel jack as feeding point, and only the first mode is stimulated. Another thing that is very important is that the inner coaxial line must stop short of the opposite wall of the guide or touch side walls to prevent mismatch, this is because in a regular rectangular waveguide the impedance is much bigger than the one from the coaxial cable. [17] The model is simulated in a range from 0.3 GHz to 3 GHz.

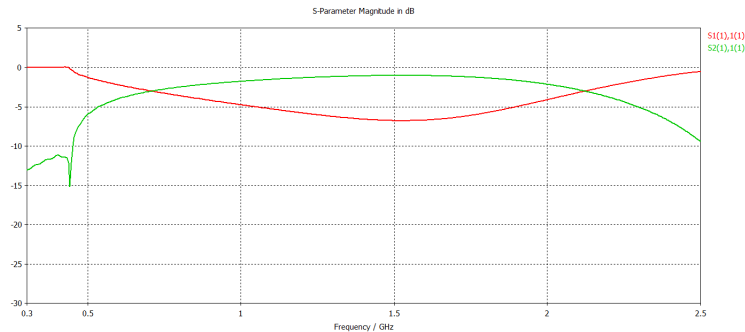


Figure 21: Reflexion factor 1

This figure shows the reflection factor $S_{1(1),1(1)}$ in red, and the sequence of the ground mode in green. The reflection factor is not reaching the desired -10dB . This means that the wave is not being transmitted correctly, it is being mostly reflected. This can be seen more clearly in the smith chart from the following figure.

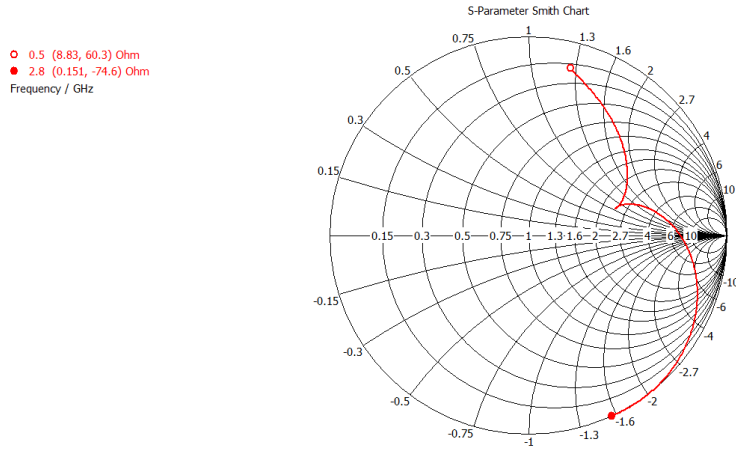


Figure 22: Smith chart, reflection factor 1

The next important step to get a better reflection factor is to determine the optimal location for the feeding point. The distance z_1 from the back side of the waveguide to the center of the panel jack is used as a variable. A series of simulations are done varying z_1 starting at the back of the waveguide and ending at the the front. The following tables shows the reflection factor for the different values of z_1 in dB and in the smith diagram.

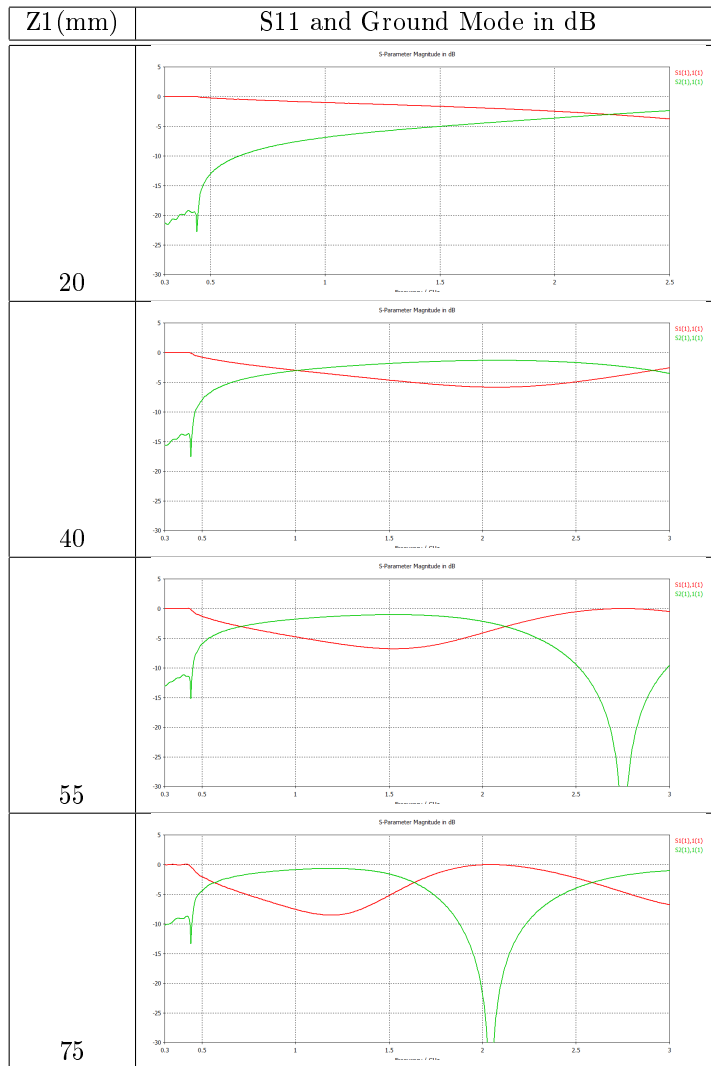


Table 7: S11 and Ground Mode Depending on Position of the Feeding Point

Z1 (mm)	S11 and Ground Mode Smith
20	
40	
55	
75	

Table 8: S11 and Ground Mode Depending on Position of the Feeding Point

In these results two different phenomenons can be observed. The first one is that the closer the feeding point is to the front of the waveguide, the sooner the ground mode signal has a total reflection, meaning that the bandwidth gets smaller every time. The reflection factor gets better each time the feeding point gets moved to the front, but as said before the bandwidth gets smaller. From Table 7 it can be noticed that the best reflection factor is at $z1 = 100mm$ but it is also shown that the ground mode makes a jump or is reflected at $1.6GHz$. The problem with the reflection factor is not solved with the optimization of the position of the feeding point, but it serves as a tuning parameter. The optimal position in this case would be $z1 = 55mm$ because even though the reflection factor is not under $-10dB$, it at least has a ground mode being transmitted correctly up to $2.5GHz$. Other methods to optimize the reflection factor are still needed.

3.3.1 Optimization With a Back Chamber

In the paper “Broad-banding coax-to-ridged-waveguide transitions”[14] it is suggested that a back chamber behind the feeding point should be built to reduce the reflection factor. A back chamber is added in the model in CST-Studio, and simulated at first with a depth of $3mm$. The depth is then iteratively increased till $50mm$ without any considerable change in the reflection factor. The following figure shows the model with the back chamber.

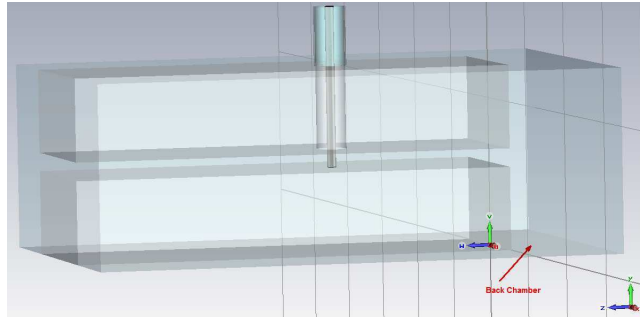


Figure 23: Waveguide Model with Back Chamber

3.3.2 Optimization With the Help of Microwave Office (AWR Design Environment)

It is known that coaxial cables work on higher frequency as a waveguide. The goal is to have a smooth transition from the feeding point to the waveguide. The characteristic impedance is determined by the size and spacing of the conductors and the type of dielectric used between them. For an ordinary coaxial cable, the characteristic impedance depends on the material and dimensions of the inner and outer conductors, and on the characteristics of the dielectric material between the inner and outer conductors. To optimize the reflection factor, the corresponding optimal dimensions must be found. The coaxial cable is represented schematically by a series of capacitors and inductance. A variation of the diameter of the outer conductor is represented by making the circuit more capacitive or inductive. A simple representation of this is shown in figure .

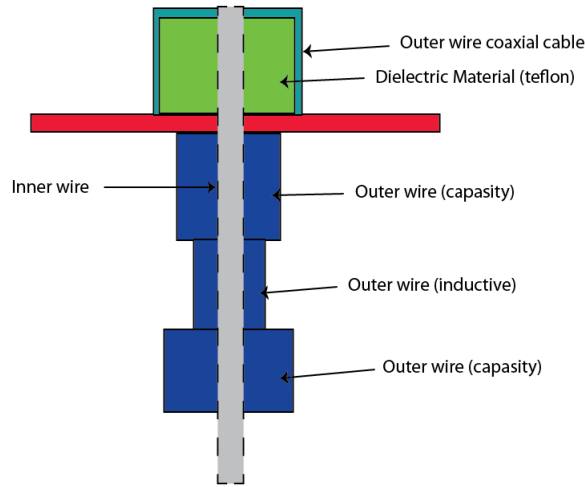


Figure 24: Representation of a Coaxial Cable

One of the special characteristics of CST Microwave Studio is that it can export the current model of the waveguide in a format called TOUCHSTONE which can also be read by AWR Design Environment. The model is interpreted as a two port system. Port 1 has a characteristic impedance of 50Ω and port two has the characteristic impedance of the waveguide, 382Ω . The system is shown in Figure 25

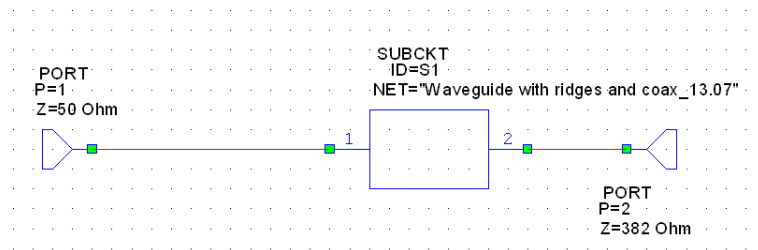


Figure 25: Waveguide Representation in AWR Design Environment

In the CST model port 1 gives a signal at the top of the top ridge, point $p1$ shown in Figure 26. Crucial to the optimization of the reflection factor is to analyze what goes on at the bottom of the top ridge, point $p2$. This is the point where the wave actually goes into the waveguide. To consider the reflection factor at point $p2$ a fictitious coaxial line is added to the original model after port 1 with a negative length of the height of the ridge. By doing so, port 1 is “moved” to point $p2$, making it possible to see what is actually going on with the reflection factor at this point. Figure 26 shows $p1$, being the point where the CST model feeds the waveguide, and $p2$, being the point that has to be analyzed.

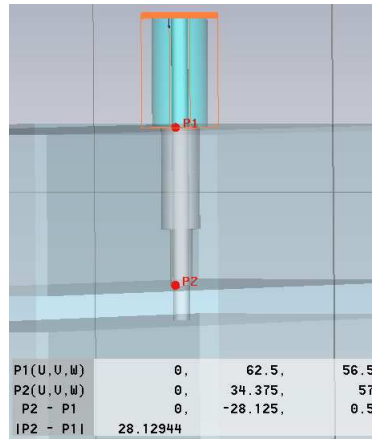


Figure 26: Different Feeding Levels of Port 1

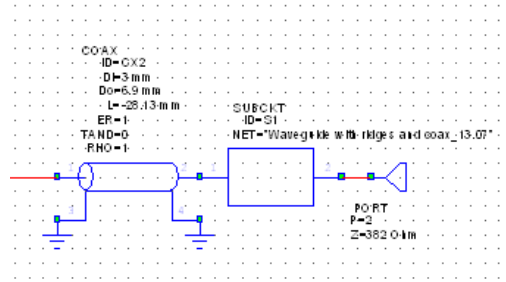


Figure 27: Representation of p2 in AWR

Notice that the length of the coaxial line is -28.13 mm. That is exactly the distance from p1 to p2. Using this configuration the optimization of the reflection factor is done by first adding two coaxial lines to the AWR model. These two lines shown in the schematic of Figure 28 are the ones going up to point p1. The first line has the variables D1 for the diameter and L1 for the length. The second coaxial line has the variables D for the diameter and L for the length.

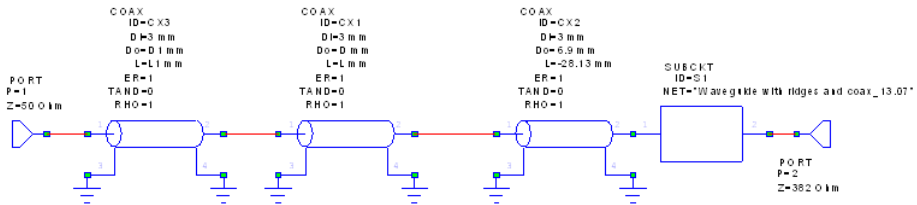


Figure 28: Schematic with Coaxial Lines

AWR is used to optimize the values for these four variables with a method called “Pointer Robust Optimization”, leaving the waveguide with the best possible

reflection factor. After the optimization the values for the variables are the following:

- $D1 = 7.73$ mm, $L1 = 20.3$ mm
- $D = 4$ mm, $L = 8.5$ mm

The following figures show the reflection factor in smith diagram and in dB . Both of them compare the initial reflection factor to the optimized one. Schematic 1 being the exported model from CST, and schematic 2 being the optimized one.

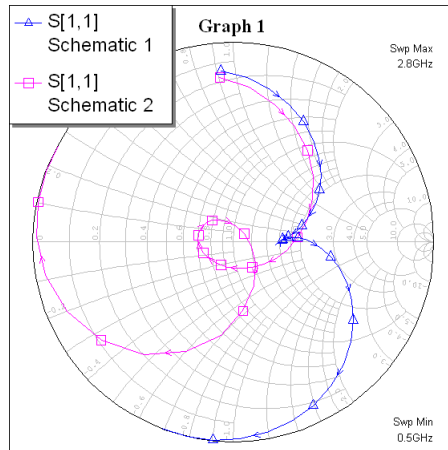


Figure 29: Smith Diagram for the Optimized Coaxial Dimension

Figure 29 shows clearly the difference between both reflection factors. The optimized one shown in red has a trajectory in the desired bandwidth around the point of total adaptation $\frac{Z}{Z_L} = 1$, in which the reflection factor $r = 0$. It does not reach the total adaptation but as shown in Figure 30 the reflection factor is under $-10dB$ in the range from $0.894GHz$ to $2.291GHz$.

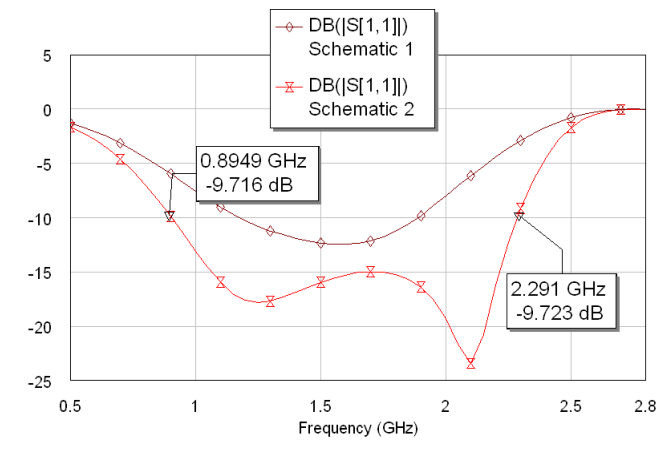


Figure 30: Reflection Factor in dB for the Optimized Coaxial Dimension

Table 9 shows, with help of smith diagrams, how the performance of the antenna changes by simply changing one of the diameters in the coaxial cable.

Diameter D1 (mm)	Reflection Factor (Smith)
0.5	
7	
12	

Table 9: Reflection Factor With one Variable Diameter

By looking at the smith diagrams, one can notice that when the diameter of the coaxial cable is reduced, the curve of the reflection factor goes to the lower part of the smith diagram, meaning that the coaxial cable has more inductive characteristics. On the other hand, when the diameter is increased, the whole curve moves up to the upper part of the smith diagram, making it capacitive. The same procedure is tried with 3 different diameters for the coaxial cable. The results shows a gradual improvement, but the idea is set aside due to constructive reasons since the diameter from the middle part was bigger than the others, making it almost impossible to drill it in the ridges.

The model is adjusted with the new diameters and simulated in CST. For building purposes, the diameter of $D1 = 7.73$ mm is changed to 8mm . The model is also simulated with this change obtaining similar results. The resulting waveguide has a bandwidth of 1.4GHz in the range from 0.9GHz to 2.3GHz . In figure 31 and 32, the results for the reflection factor computed by CST are shown, displaying almost the same results as in AWR.

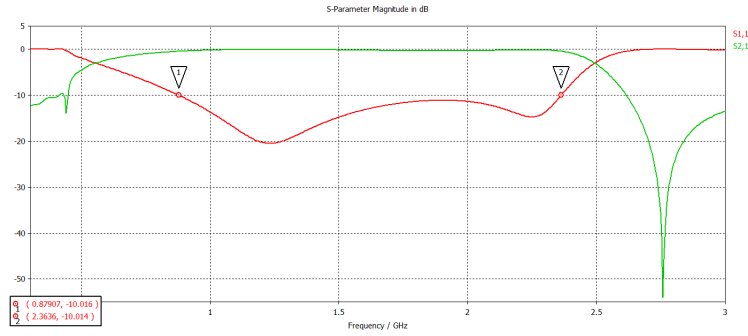


Figure 31: Reflection Factor in dB in CST after Coaxial Optimization

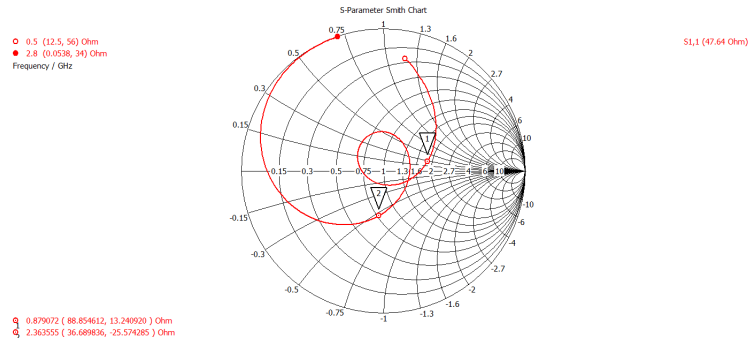


Figure 32: Reflection Factor in Smith in CST after Coaxial Optimization

3.3.3 Other Methods of Optimization

In Section 3.3.1 it was mentioned that the reflection factor could be reduced even more by adding a back chamber to the waveguide. Initial tests with the back chamber were not satisfactory, even though this technique has proven effective in previous works. A change in the ridges proves to have positive results, after many experimental variations. Instead of building a complete back chamber behind the ridges, part of the ridges are cut off behind the feeding point as shown in Figure 35. There are 3 parameters for the parts being cut out from the ridges. The first one is the distance to the back wall, the second one is the distance to the feeding point, and the third is the height of the portion being cut off. A systematical analysis is done to lower the reflection factor by changing the dimensions of the cut out part. After optimization, an increase of 0.69GHz in the bandwidth can be appreciated in Figure 33 when compared with 31. This is an increase of 50% in comparison to the waveguide without this change. The

reflection factor is under $-10dB$ for the range of $0.54GHz$ to $2.63GHz$, meaning it has a bandwidth of $1.9GHz$.

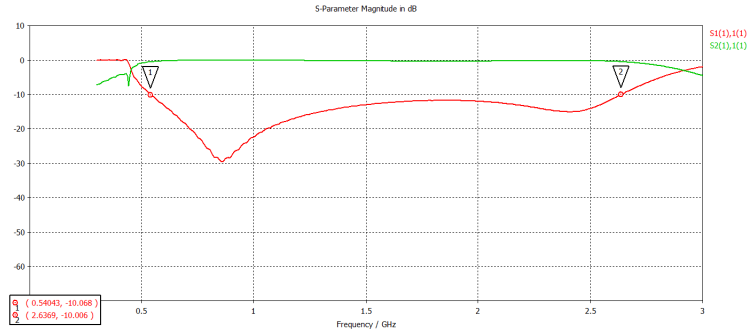


Figure 33: Reflection Factor in dB After first Optimization in the Ridges

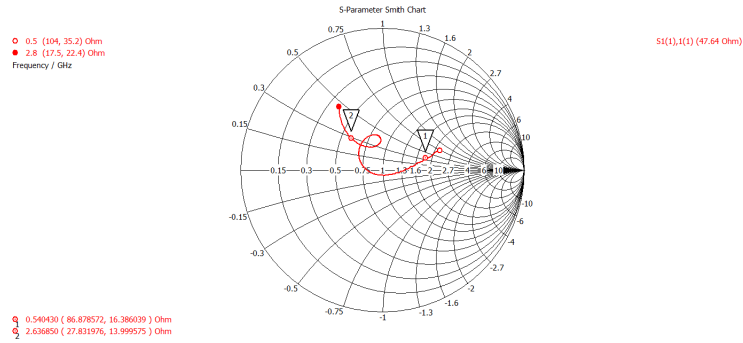


Figure 34: Reflection Factor in Smith After First Optimization in the Ridges

The considerable improvement caused by this change led to more experiments to further decrease the reflection factor in the waveguide. A second portion is consequently cut out of ridge leading to an increase in bandwidth of $0.2GHz$. With this second change, the waveguide operates with an adequate reflection factor in the range from $0.53GHz$ to $2.64GHz$. The following figure shows the new model of the waveguide with its changes.

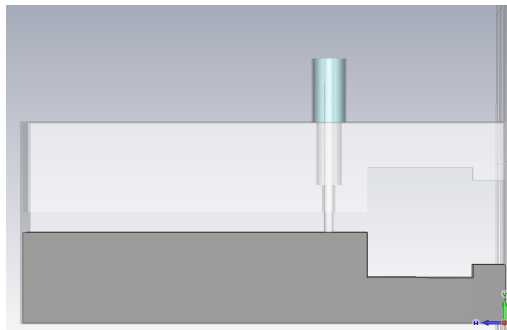


Figure 35: Waveguide Model with Changes in the Ridges

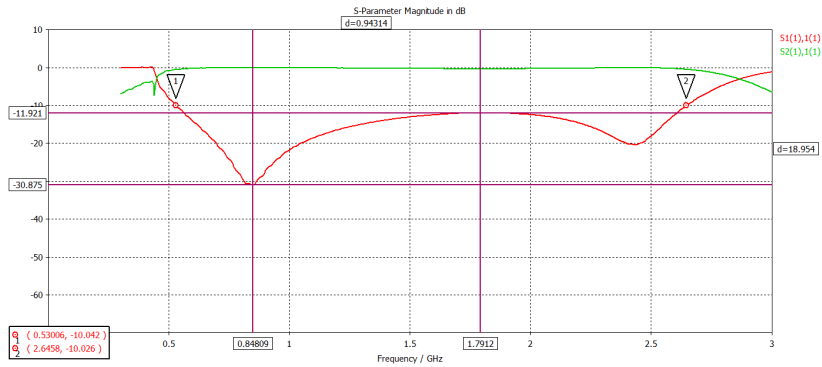


Figure 36: Reflection Factor for the Finished Waveguide

Figure 36 shows the final result for the reflection factor after all optimizations. At the frequency 0.84GHz , the reflection factor is at -30dB at its lowest point, and at 1.79GHz with -11.92dB at its highest. The reflection factor is therefore under -10dB throughout the whole desired bandwidth. With these characteristics, the horn can be added to the waveguide. To complete the analysis of this waveguide, Figure 37 shows the VSWR, which is between 1 and 2 throughout the whole bandwidth. This means according to table 2 that the reflection factor is between 0 and 11 %.

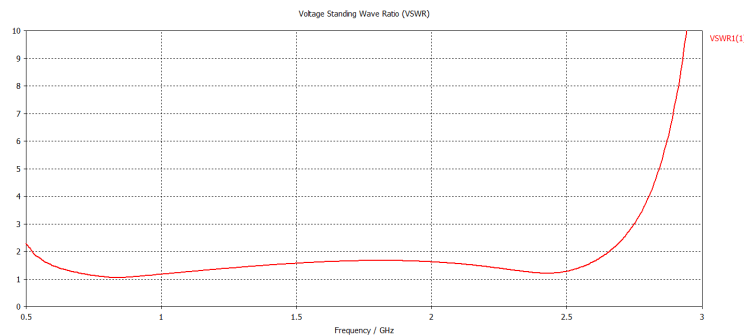


Figure 37: VSWR from the Finished Waveguide

3.4 Waveguide with Ridges and Horn

The last piece of the antenna is the horn. A simple model of a horn antenna with the following characteristics was made to analyze its attributes:

- Material: PEC (perfect electric conductor)
- Length: 300 mm.
- Height: 200 mm.
- Width: 400 mm.

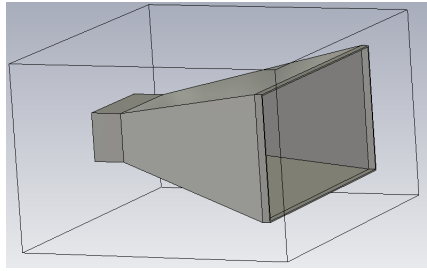


Figure 38: Model of a Simple Horn Antenna

This time, only one port with only one mode was used at the back of the waveguide. The purpose of this simulation was simply to get a feeling of the general behavior of the horn antennas. On the following graphics the gain and reflection factor are shown. Notice that the antenna is near to reflection free, with the exception of a small range from 0.8 GHz to 1 GHz. Knowing this, the waveguide that was design on the sections before can be integrated.

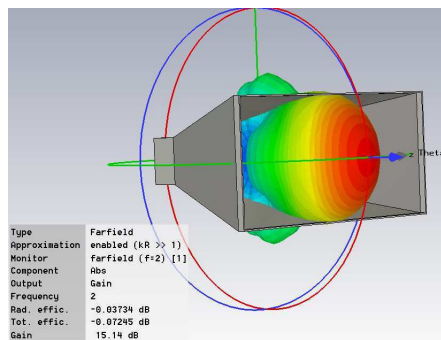


Figure 39: Gain of the Experimental Horn

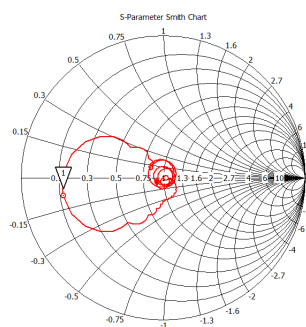


Figure 40: Reflection Factor in Smith for the Experimental Horn Antenna

3.4.1 Integration of the Waveguide and Horn

The designed and optimized waveguide is now integrated with the horn. The length, width and height of the horn are not optimized at this point. To test

how the antenna behaves with the horn, ad hoc dimensions are chosen for the horn. The model is once again simulated obtaining poor results for the reflection factor, due to the rough transition between the ridges of the waveguide and the horn. The abrupt transition from waveguide to horn, and from horn to free space, can lead to a reflection from the fed wave and to the stimulation of unwanted wave modes. The ideal transition would be from 50Ω at the beginning of the feeding point, to 377Ω at the aperture of the horn antenna which is the field wave resistance in a free space. To reach this, it is essential to have ridges in the horn that match up with the ones from the waveguide and end with an exponential behavior at the opening of the horn. According to [13] the basic function for the horn ridges can be described as:

$$S(z) = ae^{bz} + c \quad (18)$$

in which b is an independent variable and a and c are determined by the initial and end points of the exponential profile.

Equation 18 is modified to change its shape according to modifications done to the shape of the horn. The modified equation is:

$$S(z) = b_1 * e^{a_1 * z} + b_2 \quad (19)$$

where

$$b_1 = \frac{(h_1/2 - d/2)}{(e^{a_1 * l} - 1)} \quad (20)$$

and

$$b_2 = d/2 - b_1 \quad (21)$$

The only independent variable in the equation is a_1 . A tool from CST Studio is used to optimizes a desired characteristic of the antenna by changing a decision variable. In this case, a_1 is the decision variable used to optimize the antenna's directivity. After optimization, the CST tool established the value at $a_1 = 0.008$. The horn with the ridges is shown in Figure 41 .

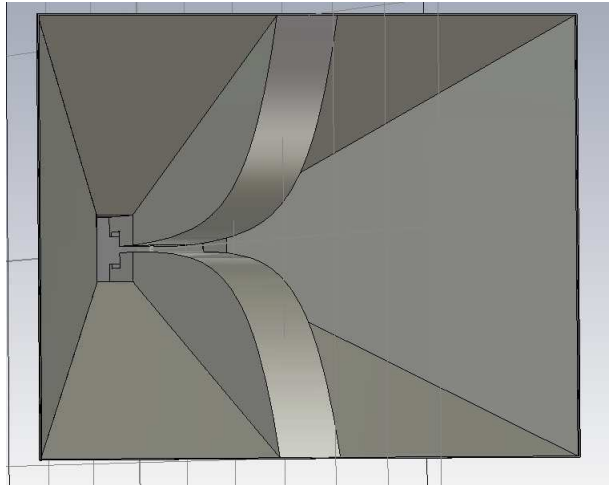


Figure 41: Curvature of the Horn Ridges

As stated in [16], smaller ridges in the horn lead to bigger losses due the fast transition to free space. Notice that the ridges in the horn have a linear behavior at the beginning and near to the end an exponential one.

After optimizing the horn ridges, the dimensions of the horn itself have to be optimized. The optimization of the horn is done with help of Figure 13. The wavelength corresponding to an operating frequency of $1.5GHz$ is approximately $20cm$. For a chosen $L = 60cm$ the ratio $\frac{L}{\lambda} = 3$. The maximum gain of $17dB$ with $h = b_h = 500mm$ is read from Figure 13.

The measurements and comparisons of the completed antenna are analyzed in Section 4.

For construction purposes, the height of the horn was reduced to $h = 400mm$ having neglectable effect on the antenna.

3.4.2 Finished Model and its Dimensions

The completed model is shown in the following figures with all the dimensions and their descriptions.

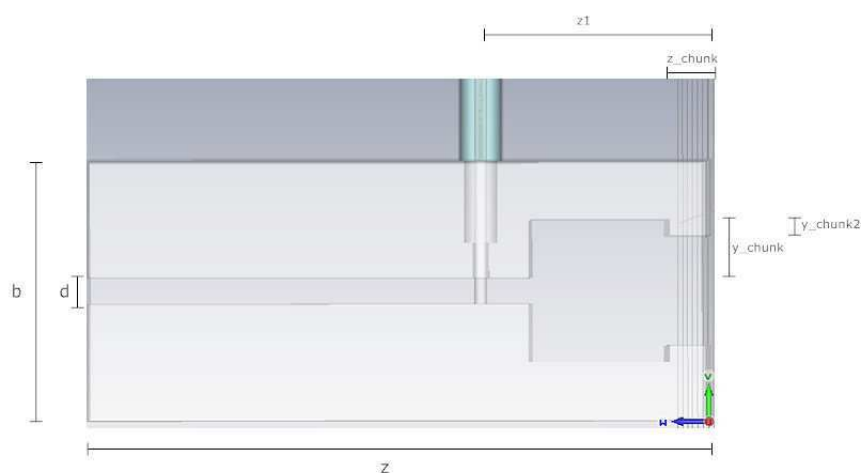


Figure 42: Waveguide from the Side

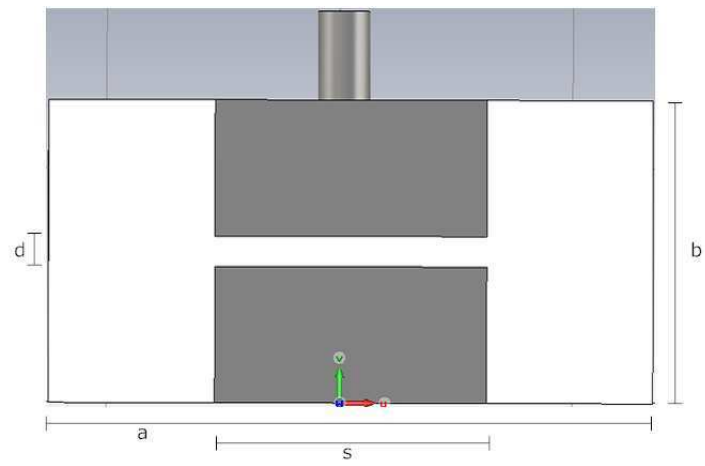


Figure 43: Waveguide from the Front

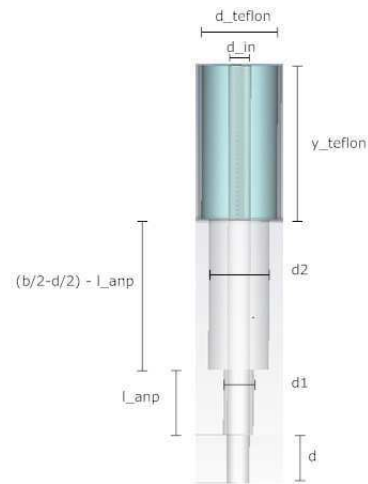


Figure 44: Coaxial Feeding Point

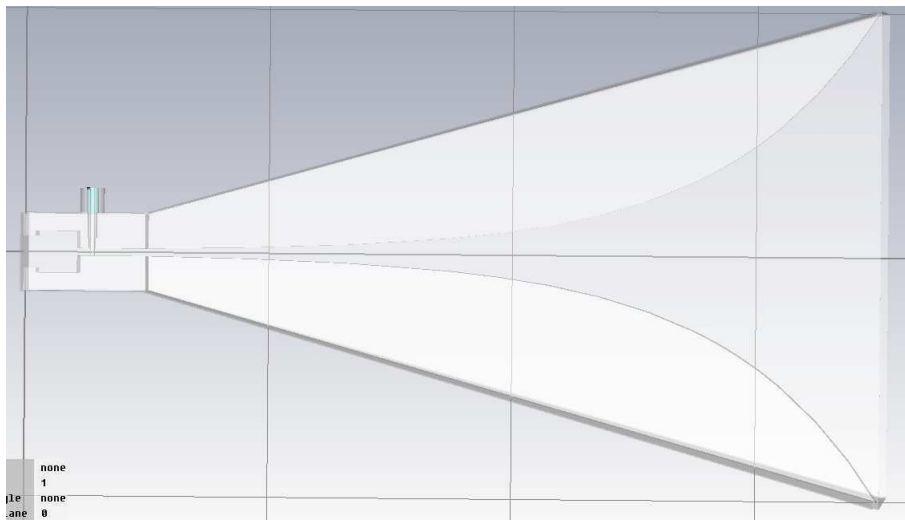


Figure 45: Complete Model from the Side

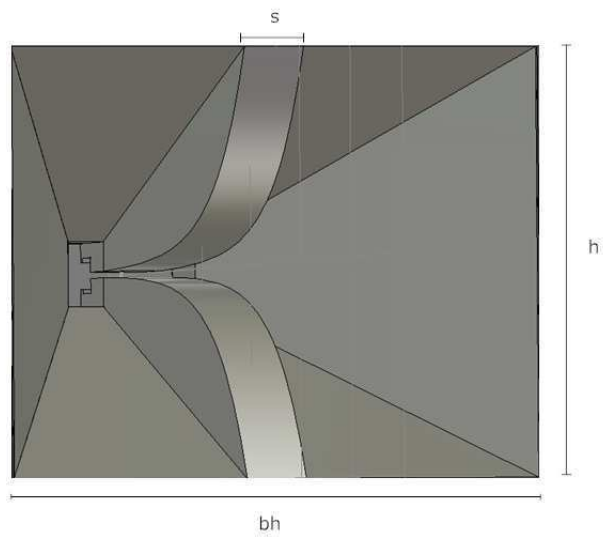


Figure 46: Complete Model from the Front

Variable	Value	Description
a	125 mm	Width of the waveguide
a1	0.008	Optimized variable for the horn ridge curve
b	62.5 mm	Height of the waveguide
bh	500 mm	Width of the horn
d	$0.1*b$	Space between waveguide ridges
d_inn	3 mm	Inner coaxial line diameter
d_teflon	10 mm	Diameter from the teflon in coaxial line
d1	4 mm	Diameter for optimized coaxial line
d2	8 mm	Diameter for optimized coaxial line
h	400 mm	Height of the horn
l	600 mm	Length of the horn
l_anp	8.5 mm	Length of one part of optimized coaxial line
s	$0.45*a$	Width of the waveguide ridges
y_chunk	14 mm	Height of the space 1 made in the ridges
y_chunk2	10 mm	Height of the space 2 made in the ridges
y_teflon	20 mm	Height of the coaxial line with teflon
z	100 mm	Length of the waveguide
z1	55 mm	Distance from the center point of the coaxial line to the back of the waveguide
z_chunk	10 mm	Distance from the back of the waveguide to the space made in the ridges

Table 10: Dimensions for the Complete Model

4 Measurements and Simulation

After concluding the modeling of the antenna with a satisfying result, the antenna is put to the test to determine all its characteristics and it is also compared with a commercial antenna to know its strengths and weaknesses.

4.1 Antenna Characteristics

Measurements of the feed horn radiation pattern and the absolute gain or directivity within the $0.4\text{-}2.7\text{GHz}$ are carried out with CST Studio. The strength of the signal transmitted by the antenna is a function of the angle at which it is transmitted. Directivity is calculated as a ratio between the power in the direction the antenna is transmitting and the average power (spherical) of the transmission. The minimum directivity of the antenna modeled in this thesis is set at 10dBi . Simulation shows that this value is not only reached, but outperformed throughout the whole bandwidth. The following figures show a 3D simulation of the directivity from the antenna at different frequencies.

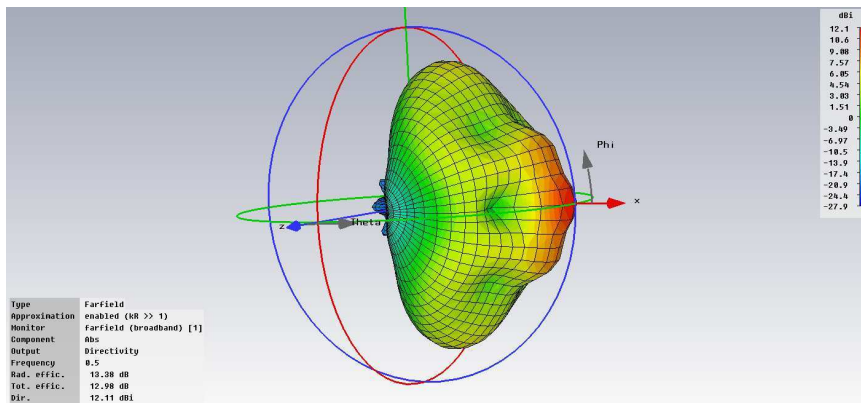


Figure 47: Directivity at 0.5 GHz

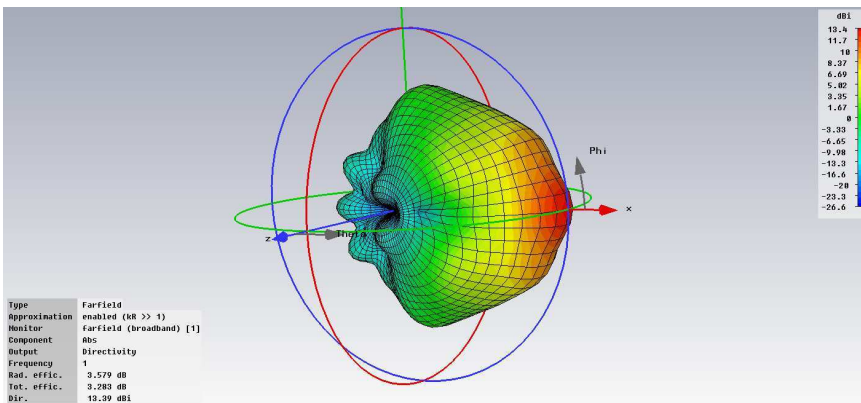


Figure 48: Directivity at 1 GHz

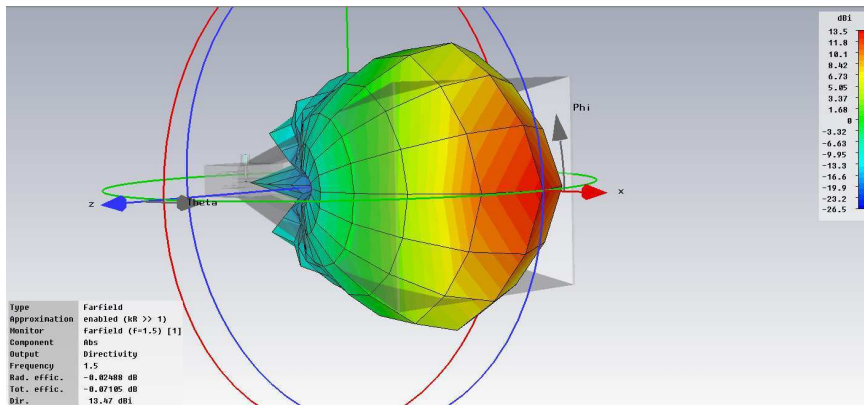


Figure 49: Directivity at 1.5 GHz

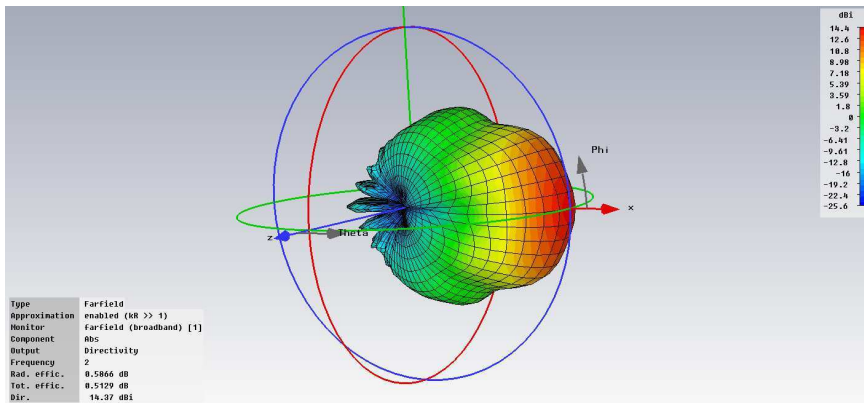


Figure 50: Directivity at 2 GHz

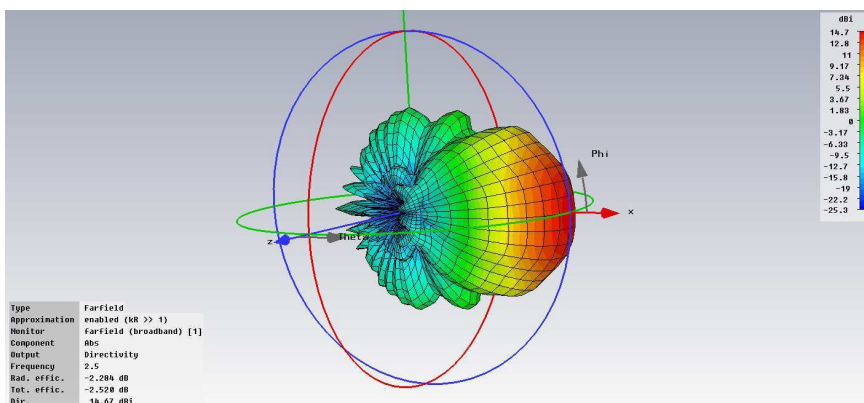


Figure 51: Directivity at 2.5 GHz

Notice that for the whole bandwidth, the radiation pattern looks as expected from a typical horn antenna. It has one dominant main lobe and small side

and back lobes. The highest directivity is in the range from 2 to 2.5GHz at 14.4dBi, although the directivity in the rest of the bandwidth is satisfactory at 13.4dBi. In order to analyze the radiation pattern in detail, the results are displayed in a two-dimensional polar E and H plane. The antenna is modeled in the x-direction, so to be able to observe the H-plane, Φ is set to 0° and Θ is varied. To be able to observe the E-plane, Θ is fixed 90° and Φ is varied. This can be best appreciated in Figure 49. Figures 52 to 56 show the E-plane of the radiation pattern.

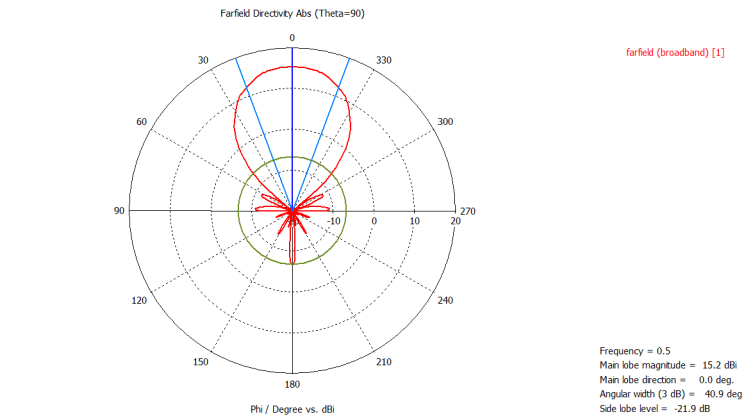


Figure 52: E-Plane at 0.5 GHz

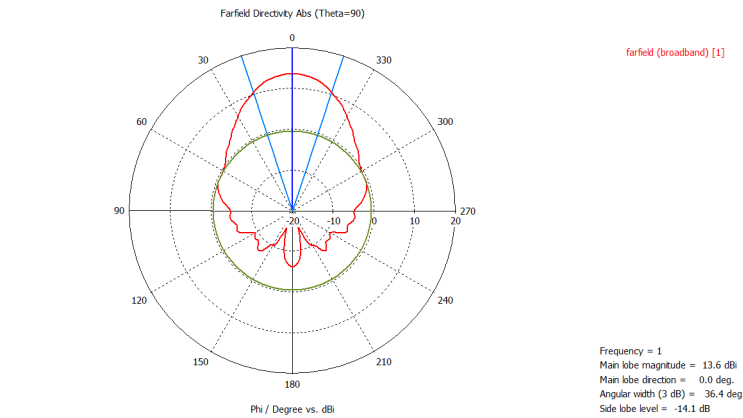


Figure 53: E-Plane at 1 GHz

4 MEASUREMENTS AND SIMULATION

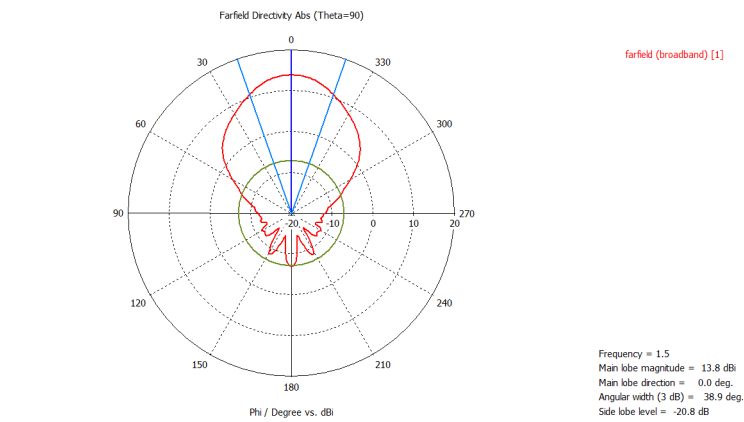


Figure 54: E-Plane at 1.5 GHz

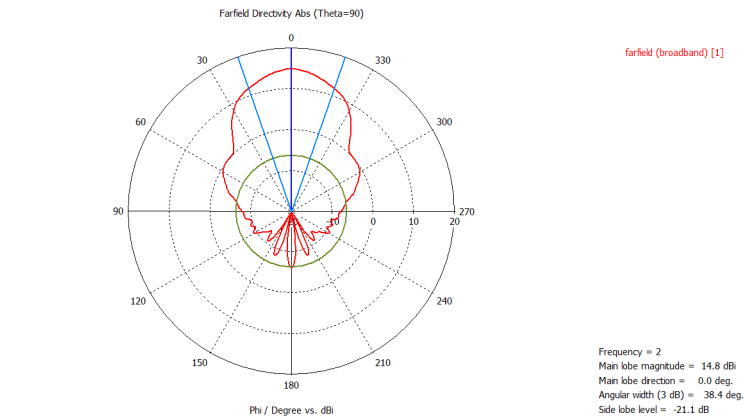


Figure 55: E-Plane at 2 GHz

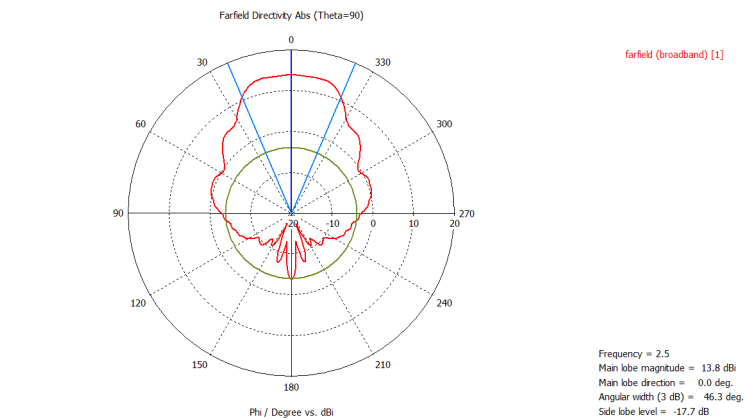


Figure 56: E-Plane at 2.5 GHz

By looking at the resulting diagrams, one can see that the antenna has a good radiation in the E-plane. The E-plane half-power beamwidth remains at 36° or more through out the whole simulation, and the side and back lobes are very small, meaning that most of the radiated energy from the antenna is going in the direction of the main lobe. A pattern degradation does not take place in the range from 0.5 to $2.7GHz$.

Figures 57 to 61 show the H-plane of the radiation pattern.

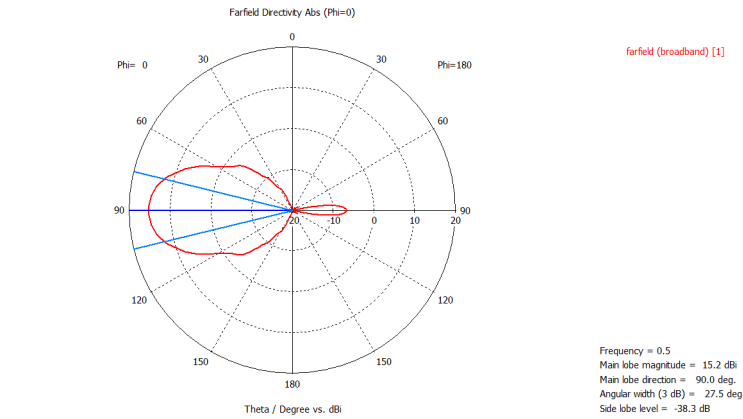


Figure 57: H-Plane at 0.5 GHz

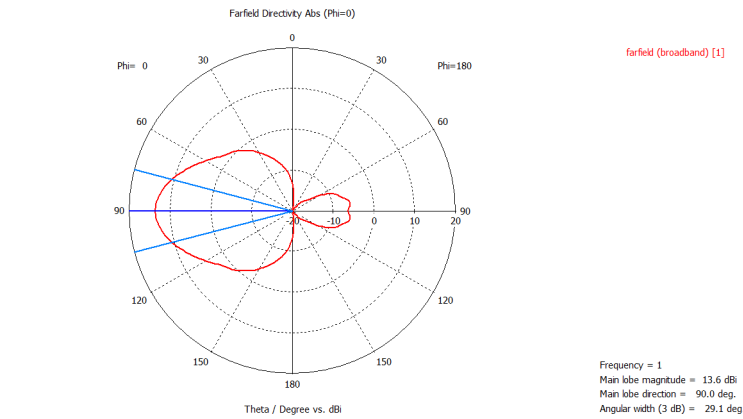


Figure 58: H-Plane at 1 GHz

4 MEASUREMENTS AND SIMULATION

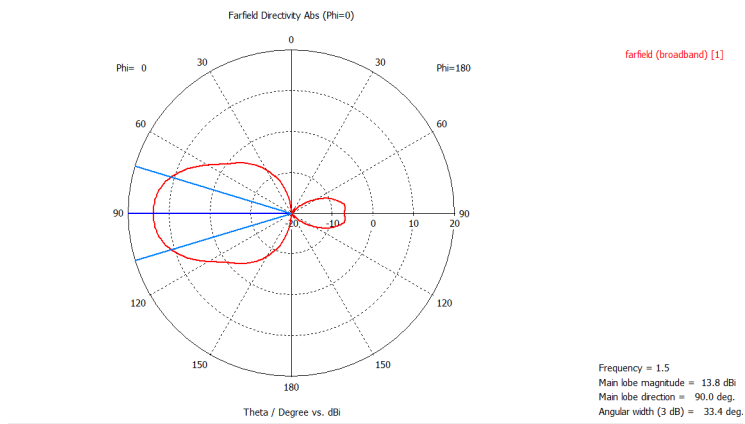


Figure 59: H-Plane at 1.5 GHz

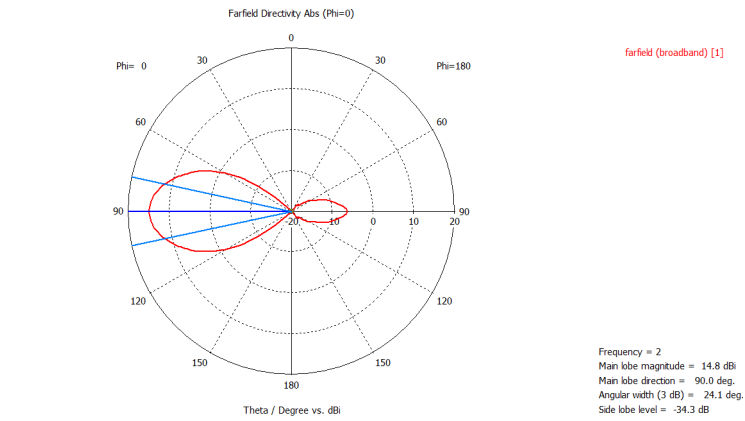


Figure 60: H-Plane at 2 GHz

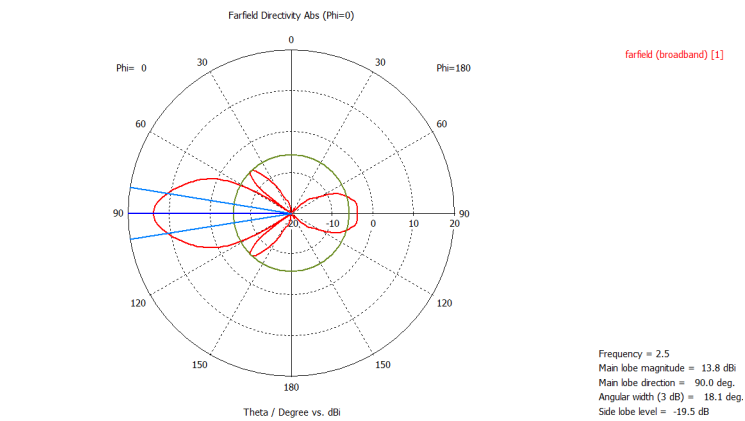


Figure 61: H-Plane at 2.5 GHz

The half-power beamwidth gets as low as 18° by a frequency of 2.5GHz . This would be a problem if the antenna had a multiwave propagation in which some modes would travel along the H-plane, but this particular model just sends a TE_{10} mode wave, which travels in the E-plane. Figure 62 displays the directivity versus the frequency in the whole bandwidth.

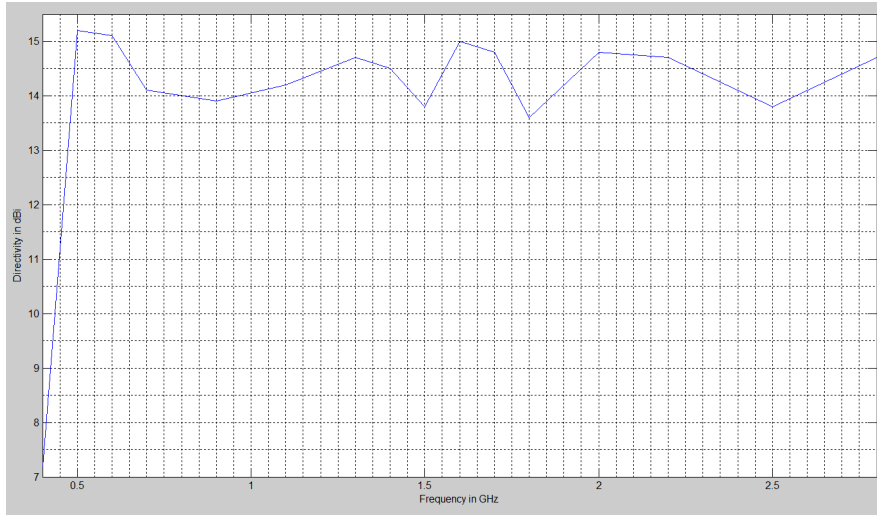


Figure 62: Directivity in the Frequency Range 0.4-2.8 GHz

The next antenna characteristic that has to be taken into account is the VSWR, and the reflection factor. The VSWR, which can be derived from the level of reflected and incident waves, is also an indication of how closely or efficiently an antenna's terminal input impedance is matched to the characteristic impedance of the transmission line. Figure 63 shows the VSWR and Figures 64 and 65 show the reflection factor in dB and Smith form.

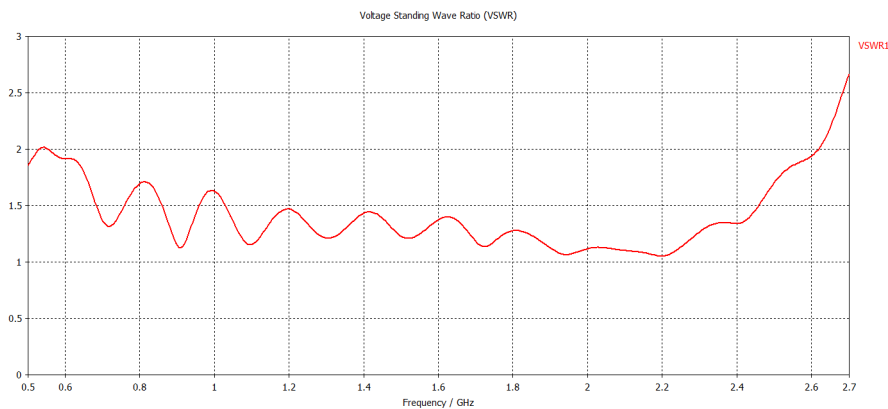


Figure 63: VSWR from the Complete Model

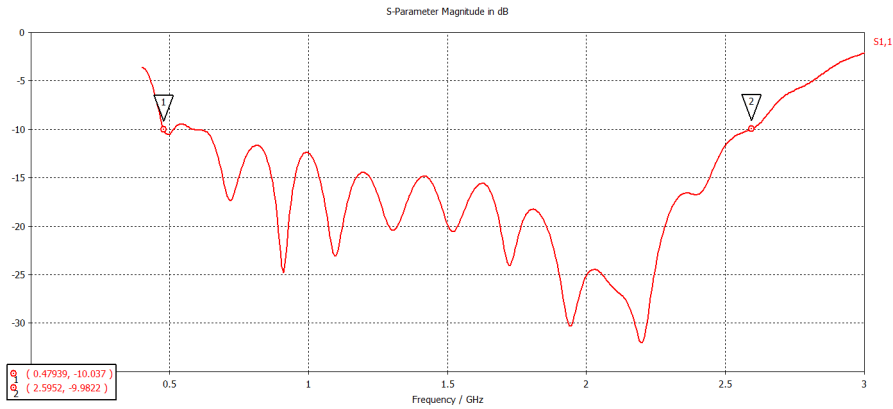


Figure 64: Reflection Factor from the Complete Model in dB

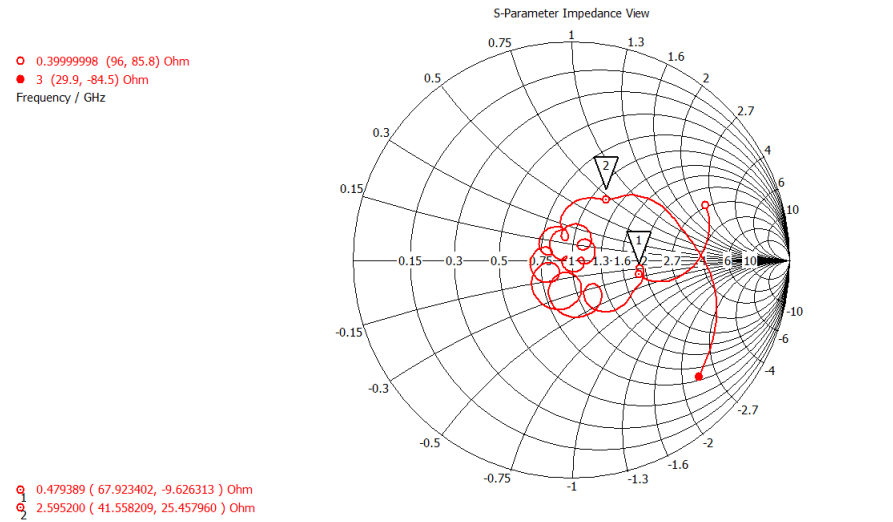


Figure 65: Reflection Factor from the Complete Model in Smith Diagram

The resulting VSWR is through out the whole bandwidth under 2:1, meaning that it has a reflection factor under 11% and a transmission loss of no more than 0.34dB. The reflection factor is under $-10dB$ in the range from 0.47GHz to 2.67GHz.

4.2 Comparison with the Lindgren 3119

The Lindgren Model 3119 is a top product from one of the leading companies in this area. It is a double ridged waveguide horn with a working frequency range from 400MHz to 6GHz. It has a impedance of 50Ω and a type N connector. The physical dimensions of this antenna are smaller than the antenna modeled in this thesis, since the Lindgren was designed for much higher frequencies. Figure 66,67, and 68 show the comparison between both antennas' Directivity

and VSWR in the range from 0.4GHz to 6GHz.

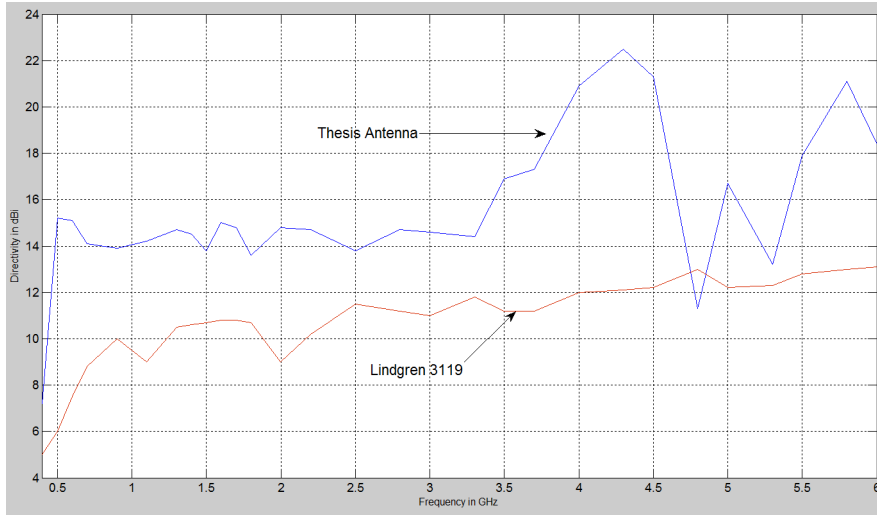


Figure 66: Directivity Comparison between Thesis's Antenna and Lindgren 3119

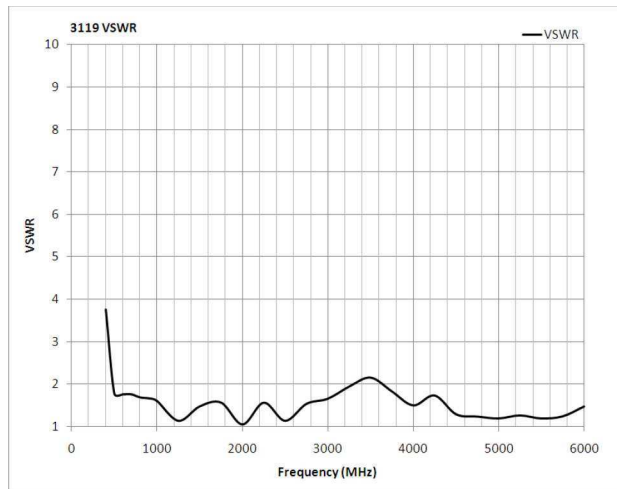


Figure 67: VSWR from the Lindgren 3119

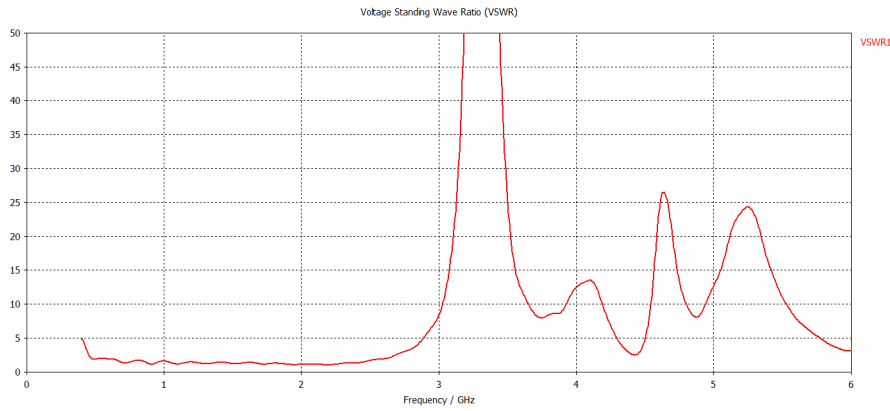


Figure 68: VSWR from Complete Model in the Range from 0.4 to 6 GHz

Figure 66 shows the directivity of the design model in blue, and the directivity from the Lindgren 3119 in red. The designed model of this thesis has a greater directivity throughout the whole frequency range, but has a considerably worse VSWR for frequencies greater than 3GHz . After looking at the results of the reflection factor in this range, it is clear that the efficiency of the modeled antenna rapidly declines after 3GHz . On the other side, this antenna was not designed for this frequencies, and after comparing both antennas, it is possible to say that the modeled antenna has a better performance in the range from 0.4GHz to 2.8GHz than the Lindgren 3119. It maintains a 40% increase in the directivity throughout this range, and both VSWR are almost equal.

5 Conclusion and Further Work

Thanks to the simulation with programs like CST Studio , it is possible to design and prove any antenna. This process is made easier by different systematical methods that allow to get great results at the end. It was crucial to maintain an order in the optimizations of each component. The antenna designed in this thesis possesses a low VSWR across its operational frequency band. It has a high and uniform gain and radiation pattern with a very low reflection factor. Its bandwidth from 0.5 GHz to 2.67 GHz meets the requirements set by the university, and some of its characteristics exceeded the expectations.

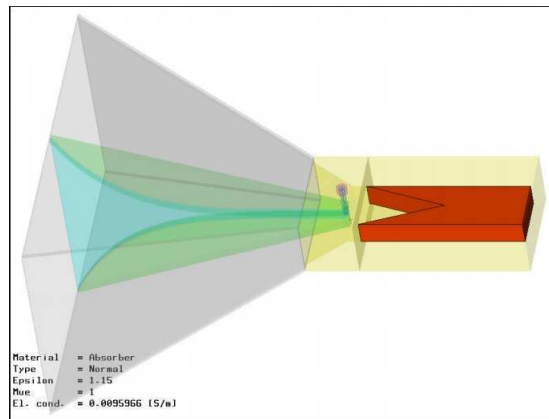


Figure 69: Further Changes for the Antenna

There are still some changes that can be done to this model that could not be implemented because of time. Two very interesting changes that can be done are explained in the Paper [1]. The first one is to integrate a dielectric which partially fills the gap between the ridges. This is done in order to decrease the lower frequency limit and by doing so increasing the frequency range of the antenna. The second change is to integrate a wave absorber at the back of the waveguide in order to get rid of the unwanted reflections in the waveguide. Figure shows more less how this should be done.

References

- [1] A. Jöstingmeier A. Teggatz and A. S. Omar. A new tem double-ridged horn antenna for ground penetrating radar applications. *Institute for Electronics, Signal Processing and Communications*. 5
- [2] antenna theory.com. Field regions. 1999. Version 2. 2.1.2
- [3] Constantine A Balanis. *Antenna Theory*. Wiley, 2005. Page 27. 2.2.2.1
- [4] Constantine A Balanis. *Antenna Theory*. Wiley-Interscience, 2005. Chapter 2.6 page 44. 2.2.2.2
- [5] Constantine A Balanis. *Antenna Theory*. Wiley-Interscience, 2005. Chapter 2.9 page 66 With the directivity characteristics and the directivity diagrams you are able to determine how strong the antenna bundles the radiation on a sector. 2.2.2.2
- [6] Constantine A Balanis. *Antenna Theory*. Wiley-Interscience, 2005. Chapter 2.11 page 70. 2.2.2.3
- [7] Constantine A Balanis. *Antenna Theory*. Wiley, 2005. chapter 2.13, page 80. 2.2.2.5
- [8] <http://www.phys.hawaii.edu/anita/new/papers/militaryHandbook/waveguid.pdf>. Microwave waveguides and coaxial cable. 2.3.2
- [9] <http://www.phys.hawaii.edu/anita/new/papers/militaryHandbook/waveguid.pdf>. Microwave waveguides and coaxial cable. 2.3.5
- [10] Klaus W. Kark. *Antennen und strahlungsfelder*. 2010. chapter 14.3, page 353. (document), 12
- [11] Professor Dr. Ing. Klaus Lange. *Taschenbuch der Hochfrequenztechnik*, volume Band 2. Springer-Verlag, 1992. 2.3.1
- [12] Professor Dr. Ing. Klaus Lange. *Taschenbuch der Hochfrequenztechnik*, volume Band 2. Springer-Verlag, 1992. chapter 4.3 section K24. 2.3.3
- [13] Jali Rashed-Mohassel Majid Abbas-Azimi, Farrokh Arazm. Design of a new broadband emc double ridged guide horn antenna. 3.4.1
- [14] P. J Muenzer. Broadbanding coax-to-ridged-waveguide transitions. 1964. 3.3.1
- [15] David M. Pozar. *Microwave Engineering*. John Wiley & sons, Inc, 2005. 2.3.2
- [16] Holger Stolzenburg. Modellierung und simulation eines breitbandigen hornstrahlers mit der software cst-studio. 2010/2011. 3.4.1
- [17] R. Pendleton T. Rizawa. Broadband coax-waveguide transitions*. *Stanford Linear Accelerator Center, CA 94309, USA*. 3.3

Hereby, I declare that I produced the present work myself only with the help of the indicated aids and sources.

Hamburg, October 14, 2011

Carlos Silvera